The Dissertation Committee for Michele Di Pierro Certifies that this is the approved version of the following dissertation:

Optimization Of Force Fields For Molecular Dynamics

Committee:

Ron Elber, Supervisor

Peter J. Rossky

Oscar Gonzalez

William H. Press

Pengyu Ren

Optimization Of Force Fields For Molecular Dynamics

by

Michele Di Pierro, M. Physics; M.S.C.A.M

Dissertation

Presented to the Faculty of the Graduate School of

The University of Texas at Austin

in Partial Fulfillment

of the Requirements

for the Degree of

DOCTOR OF PHILOSOPHY

The University of Texas at Austin

December 2014

Dedication

To my wife Erica.

Acknowledgements

Foremost, I would like to thank my advisor Prof. Ron Elber for accompanying me on the path of becoming a scientist, constantly teaching the way.

Thanks to my committee members Prof. Gonzalez, Prof. Press, Prof. Rossky and Prof. Ren for always being available whenever needed and for their constant support.

Thanks to the faculty and wonderful staff of the Institute For Computational Engineering and Sciences; especially Ruth Hengst and Stephanie Rodriguez who helped me survive in the jungle of bureaucracy.

Finally, thanks to my fellow lab mates: Mauro Mugnai, Peter Majek, DVS Ravikant, Szu-Hua Chen, Shruthi Viswanath, Alfredo Cardenas, Serdal Kirmizialtin, Baoqiang Cao, Thomas Blom, Peter Ryumgaart, Juan Bello Rivas, Daniel Walker and Katelyn Poole for the joyful environment they provided and innumerable stimulating conversations.

Optimization Of Force Fields For Molecular Dynamics

Michele Di Pierro, PhD

The University of Texas at Austin, 2014

Supervisor: Ron Elber

A technology for optimization of potential parameters from condensed phase simulations (POP) is discussed and illustrated. It is based on direct calculations of the derivatives of macroscopic observables with respect to the potential parameters. The derivatives are used in a local minimization scheme, comparing simulated and experimental data. In particular, we show that the Newton Trust-Region protocol allows for accurate and robust optimization.

POP is illustrated for a toy problem of alanine dipeptide and is applied to folding of the peptide WAAAH. The helix fraction is highly sensitive to the potential parameters while the slope of the melting curve is not. The sensitivity variations make it difficult to satisfy both observations simultaneously. We conjecture that there is no set of parameters that reproduces experimental melting curves of short peptides that are modeled with the usual functional form of a force field.

We then apply the newly developed technology to study the liquid mixture of tert-butanol and water. We are able to obtain, after 4 iterations, the correct phase behavior and accurately predict the value of the Kirkwood Buff (KB) integrals. We further illustrate that a potential that is determined solely by KB information, or the pair correlation function, is not necessarily unique.

Table of Contents

List of Tables

List of Figures

Introduction[a]

Molecular Dynamics (MD) is a technique that makes it possible to study the dynamics and thermodynamics of molecular systems.

MD simulations are computer experiments. In a wet laboratory experiment we first prepare the material we plan to study, we then measure some property of interest for a certain interval of time. If there is some statistical noise then the longer is the interval of time the more accurate are the measurements.

In a MD simulation the measurement mimics experiment. Our sample in this case consists of a model system composed of *N* atoms. For this system we solve the equations of motion to observe how properties of interest evolve as a function of time. For equilibrium simulations we will let the system equilibrate until the properties of the system no longer change with time and then we perform the measurement as an average over a time series.

---

[a] Part of the content of this chapter was previously published in collaboration with Ron Elber in

Di Pierro and Elber (2013). "*Automated Optimization of Potential Parameters*." *J. Chem. Theory Comput.*, **2013**, *9* (8), pp 3311–3320, **DOI:** 10.1021/ct400313n

and with Ron Elber and M.L.Mugnai in

Di Pierro et al. (2014). "*Optimizing Potentials for a Liquid Mixture: A New Force Field for a tert-Butanol and Water Solution*." *J. Phys. Chem. B*, Article ASAP, **DOI:** 10.1021/jp505401m

Ron Elber supervised both works; M.L. Mugnai contributed to the adaptation of the KB theory and provided part of the simulation data.

The motion of a system of atoms is governed by the time dependent Schrödinger equation; unfortunately, the Schrödinger equation is tractable only for relatively small systems. MD consists of integration in time of the motion of a system of atoms using a Hamiltonian that is a classical approximation of the exact quantum mechanical description of the dynamics.

The motion of electrons is captured in an effective potential and the nuclei are represented as mass points. The equations of motion are therefore:

$$\ddot{x}_i = \frac{1}{m_i} \nabla U\left(x_1, x_2, x_3, ..., x_N\right) \tag{1.1}$$

for each nucleus i in the system. The potential $U(x)$ couples the motions of all the atoms and represents both the chemical bonds and the interactions between non-bonded atoms.

Clearly, the potential is a critical element of modeling matter with MD. In this thesis we will focus on a statistical mechanic formulation of ways to estimate potential parameters and the sensitivity of measured properties to the choice of these parameters.

The basic functional form for MD potentials is a summation of bonding and non-bonding terms. The non-bonding terms are represented by pair potentials: the Lennard Jones potential and the point charge Coulombic energy. The bonding terms are represented by two, three and four body potentials (bonds, angles, proper and improper torsions):

$$
\begin{aligned}
&U = \sum_b U_b + \sum_\theta U_\theta + \sum_\phi U_\phi + \sum_I U_I + \sum_{LJ} U_{LJ} + \sum_{elec} U_{elec} \\
&U_b = \frac{k_b}{2}\left(b - b_0\right)^2 \quad U_\theta = \frac{k_\theta}{2}\left(\theta - \theta_0\right)^2 \quad U_\phi = \sum_n a_n \cos\left(n\phi + \delta_n\right) \\
&U_I = \frac{k_I}{2}\left(\phi_I - \phi_{I0}\right)^2 \quad U_{LJ} = 4\varepsilon\left(\left(\frac{\sigma}{r}\right)^{12} - \left(\frac{\sigma}{r}\right)^{6}\right) \quad U_{elec} = k_{el}\frac{q_i q_j}{r_{ij}}.
\end{aligned}
\tag{1.2}
$$

For the Lennard Jones potential a mixing rule for different chemical species must be defined; OPLS[1] force field for a pair of atom types (i,j) defines $\sigma_{ij} = \sqrt{\sigma_i \sigma_j}$ and $\varepsilon_{ij} = \sqrt{\varepsilon_i \varepsilon_j}$ (another mixing rule used by other force fields is $\sigma_{ij} = \frac{1}{2}\left(\sigma_i + \sigma_j\right)$). The defined Hamiltonian depends on the set of parameters $\left\{\{k_b, b_0\}, \{k_\theta, \theta_0\}, \{k_I, \phi_{I0}\}, \{a_n\}, \{\sigma, \varepsilon\}, \{q\}\right\}$; the complete set of parameters is denoted by π.

The equations of motion are integrated in time using a time stepping algorithm. One of the simplest of the suitable algorithms is the momenta Verlet[2] algorithm:

$$
\begin{aligned}
x_i\left(t + \delta t\right) &= x_i\left(t\right) + \frac{p_i\left(t\right)}{m_i}\delta t - \frac{1}{2m_i}\nabla_i U\left(x\left(t\right)\right)\delta t^2 \\
p_i\left(t + \delta t\right) &= p_i\left(t\right) - \frac{1}{2}\left(\nabla_i U\left(x\left(t\right)\right) + \nabla_i U\left(x\left(t + \delta t\right)\right)\right)\delta t
\end{aligned}
\tag{1.3}
$$

where the x_i and p_i are the coordinate and momentum vectors of the atom i.

Momenta Verlet is a symplectic integrator[3] and therefore conserves the phase space volume.

So far we have described what constitutes a mathematical model of the molecular system under investigation; we can now use a computer simulation to compute the equilibrium and transport properties of this classical many-body system.

To measure a quantity of interest we first need to be able to express it as a function of the positions and the momenta of the particles in the system. Not all the properties that we can measure in a simulation correspond to properties that can be measured in experiments. For example, in a MD simulation we can measure the instantaneous position and velocities of all the molecules in the system. There is no wet laboratory experiment that could provide us with such detailed information. Usually, an experiment measures an average property, averaged over a large number of molecules and often averaged over the time of the experiment.

If we wish to compare equilibrium results from computer simulations and experiments we need to use averages computed using statistical mechanical ensembles. These comparisons are used to validate the results of the computer simulations and to fine-tune the computational models as well as to gain more detailed insight into the experimental measurements.

Ensemble averages are computed in MD by a time series

$$\langle O \rangle = \lim_{t \to \infty} \frac{1}{t} \int_0^t O(t')dt' \tag{1.4}$$

and are compared to the experimental value O_{exp}. If the trajectory is sufficiently long and ergodic, and is computed according to dynamics that produces the canonical distribution of coordinates (e.g. iso-kinetic ensemble[4]) then the time series can be replaced by the canonical ensemble average

$$\langle O \rangle_{(\pi,T)} = \frac{\int dx\, dp \cdot O(x,p,\pi) \mathrm{e}^{-\beta H(x,p,\pi)}}{\int dx \cdot \mathrm{e}^{-\beta H(x,p,\pi)}} \tag{1.5}$$

where H is the Hamiltonian of the system and $\beta = 1/kT$.

Predictions by MD of experimental observations have two sources of errors: (i) statistical and (ii) systematic (biased) errors. Longer simulations can reduce the statistical errors but systematic error remains. If the statistical sampling is adequate, the remaining errors are a result of inaccuracies in the potential $U(x)$. These inaccuracies can be in the functional form. For example, the use of atomic point charge models to compute electrostatic energies may be insufficient; the problem may require a better formulation of the charge density of electrons around atomic nuclei that includes polarization of the local electron clouds. Alternatively the simplified functional form of the potential may be sufficient and the cause of inaccuracies may lie in the non-optimal choice of the many parameters that characterize the potentials.

Interestingly, widely used force fields such as CHARMm[5], AMBER[6], and OPLS[1] retain highly similar functional forms. Refinements of the energy function are mostly made by adjustments of the parameters of the energy function.

The standard functional form of MD showed robustness and transferability and is the method of choice of most of simulation software. While many quantitative and qualitative observations support the validity of such MD force fields, it is certainly possible to improve its functional form. There are many ongoing efforts in this direction; the addition of polarization terms[7,8] and the addition of statistical potentials[9] are examples of such efforts.

The MD model contains thousands of parameters: the set of these parameters is what is often referred to as the force field itself. Each one of these parameters has been fitted to reproduce the equilibrium molecular geometry of model compounds using both experimental values and *ab initio* calculations in a long, manual, and labor-intensive process. These parameters are sometimes further tuned (manually) against condensed phase experimental and computational observables. The mere existence of multiple force fields means by itself that an optimal parameterization has not yet been found.

Advancements in computer power and simulation techniques continuously raise the bar of what is possible to model; systems of millions of atoms can be studied with MD[10], and the longest simulations can reach milliseconds.[11] New interesting applications are investigated and new simulation challenges are found.

As the world of molecular simulations grows in size and complexity, there is a growing demand for more accurate force fields capable of recovering subtle physical phenomena that are difficult to reproduce with simplified interaction models. The recent and continuous increase of simulation lengths allows us to compute converged statistical averages to be compared to experimental data that were inaccessible to simulations in the past.[12]

Throughout the years, considerable success has been accomplished in reproducing many experimental observables *in silico*. Only recently, however, sufficiently long

simulations have been conducted so that a careful validation of force fields against condensed phase, thermodynamic data for biological molecules is possible.

In this thesis I will develop a method for the optimization of the whole parameter set using condensed phase observables for calibration. The method is called POP [13,14] (Parameter OPtimization) and is implemented in the software package MOIL[15]. POP aims to be a useful tool for the scientist in two ways. First, in the assessment of the quality of the functional form of the model: is it possible to reproduce this specific experimental observation with the current functional form? Second, POP introduces a systematic, reproducible approach to the development of force fields in computational chemistry.

The optimization of the whole parameter set using condensed phase observables as targets is an optimization problem with specific features and difficulties. One specific difficulty is that each calculation of the condensed phase observable is computationally very expensive as many time steps are required for accurate averages (the statistical errors decrease in the best scenario as $\sqrt{t}$); a typical calculation can take days or weeks. The dimensionality of the parameter space is also generally large. To be useful, our optimization scheme is required to improve the parameter set in just a few iterations. This fact alone rules out popular optimization methods such as Monte Carlo Optimization[16] for example.

We solved the problem using a gradient-based method. While previous attempts of gradient-based optimization in MD were based on numerical differentiation, we proved that it is possible and convenient to calculate the full gradient in parameter space as a single statistical mechanical ensemble average. This is due to the fact that we know a priori the functional form of the probability distribution for any statistical mechanical

observable. This result allowed us to extend our optimization to systems that were previously intractable because of their high dimensionality.

I applied POP to different systems and aims. The first application involves structural properties of short peptides that are used to model early events in protein folding. In this particular case the agreement between experimental and computational observables is poor. Experimental techniques provide insights on structural properties of peptides and measurements are readily available. For example, the fraction of folded peptides can be measured with Circular Dichroism (CD) or Förster Resonance Energy Transfer (FRET). On the other hand, to measure the folded fraction *in silico* a large number of folding/unfolding events is required, hence the historical difficulty in simulating it.

Recent studies[17] have shown that many commonly used force fields cannot effectively reproduce the melting curve of short peptides (either β-hairpins or α-helices). The agreement with experiment is poor; in the tested cases the results of *in silico* measurements of the folded fraction were dependent on the choice of the force field. Not one of the tested force fields was able to reproduce the folded fraction as a function of the temperature for a significant temperature interval. This last result raises doubts about the ability of the current functional form of MD potentials to reproduce *in silico* the correct experimental temperature dependence. I first applied POP to the model system alanine dipeptide to test our ability to efficiently modify force field parameters; then we applied POP to the pentapetide WH5 in the attempt to reproduce the experimental melting curve. In this application we did not produce a new force field of general utility; instead we investigate the existence of a parameter set that could reproduce the temperature dependence of the folded fraction with the standard functional form of MD force fields.

The second application of POP involves liquid binary mixtures; typically the mixture will be composed of water and a solute, but not necessarily. The development of force field parameters for a small molecule that is part of fluid phase typically involves multiple stages. It involves quantum mechanical calculations (usually in gas phase) to fit molecular mechanics parameters, and condensed phase calculations to adjust intermolecular parameters so that thermodynamic properties can be reproduced.

Sometimes properties of liquid mixtures are not well reproduced by the parameters developed to describe a single component system. It is therefore desired to address liquid mixtures more directly, and to consider theories and algorithms tailored for these systems. There are a few examples of theories that capture properties of solutions in a relatively small number of parameters. The Kirkwood-Buff (KB) integrals[18] summarize a set of experimental observables characterizing liquid mixtures and are useful targets of optimization of potential parameters.[19-21]

We combine POP and the observables of Kirkwood-Buff theory to optimize potential for liquid mixtures. We use the POP method to improve the current force field for tert-butanol (TBA) in aqueous solution. Our starting point is the OPLS united atom (OPLSUA) parameters for tert-butanol,[22] and TIP3P[23] water model. We develop a new set of parameters only for tert-butanol. We retain the same water model that was tested comprehensively by now on a very large number of systems. We seek a set of TBA parameters that better reproduces the KB integrals estimated from experiments[24] over a range of different concentrations. While optimization for TBA-water mixtures according to KB integrals have been done in the past,[21] the present study is automated, producing high quality potentials, and making it possible to address questions about the uniqueness of the results.

Method[b]

POP algorithm

Definition of the problem

We denote an experimental measurement of an observable O by O_{exp}. The measured quantity corresponds to the (canonical) ensemble average of a certain function of the phase space (positions are collectively indicated by x and momenta by p) that may or may not depend on the force field parameters π:

$$\langle O \rangle_{(N,V,T,\pi)} = \frac{\int dr\, dp \cdot O(x,p,\pi) \mathrm{e}^{-\beta H(x,p,\pi)}}{\int dx\, dp \cdot \mathrm{e}^{-\beta H(x,p,\pi)}} \tag{2.1}$$

[b] Part of the content of this chapter was previously published in collaboration with Ron Elber in

Di Pierro and Elber (2013). "*Automated Optimization of Potential Parameters*." *J. Chem. Theory Comput.*, **2013**, *9* (8), pp 3311–3320, **DOI:** 10.1021/ct400313n

and with Ron Elber and M.L.Mugnai in

Di Pierro et al. (2014). "*Optimizing Potentials for a Liquid Mixture: A New Force Field for a tert-Butanol and Water Solution*." *J. Phys. Chem. B*, Article ASAP, **DOI:** 10.1021/jp505401m

Ron Elber supervised both works; M.L. Mugnai contributed to the adaptation of the KB theory and provided part of the simulation data.

The ensemble average of the observable always depends on the set of parameters π through the exponential weight, and of course it depends on the macroscopic constraints of the system (number of particles N, volume V, and temperature of the thermal reservoir in contact with the system T).

One way to validate the results of a simulation is to measure how much computed observables differ from experimental measurements. Here, we optimize the parameters in the MD force field in order minimize the discrepancy between computed and experimental observables.

Given N_O experimental observations we define our target function to be [13,14]:

$$\Theta(\pi) = \sum_{i=1}^{N_O} \left[\langle O_i \rangle_\pi - O_{\exp,i} \right]^2 \tag{2.2}$$

Other choices of the target function are possible, provided that the target function is differentiable and has a global minimum when the computed observables are equal to the experimental measurements. The optimal set of parameters is π^* such that:

$$\pi^* = \arg\min \Theta(\pi) \tag{2.3}$$

Trust Region Newton Method

The optimization problem defined in the previous section is very general but it also has some specific features due to the fact that the optimization aims to use condensed phase observables as optimization targets. These features suggest what could be a feasible approach to find the optimal parameterization and which methods are not applicable to our specific problem.

The first thing we need to consider is that calculating ensemble averages through MD is a challenging computational task that requires typical times of days to weeks to converge to the desired result. This implies that we need to minimize the target function using a minimal amount of evaluations of the target function itself. This simple consideration rules out common optimization methods like Monte Carlo Minimization or searching for the minimum by using a grid in parameter space. This first feature of our optimization problem indicates that the best possible way to find the minimum could be using a derivative-based method. The information contained in the derivatives of the target function helps move in the direction of maximum improvement of the parameter set.

The second feature we consider is the dimensionality of the parameter space. Even for relatively small systems the number of parameters is very high, typically in the range of hundreds to thousands. If we want to use a minimization scheme based on the gradient then we need to find a way to calculate it. Numerical differentiation is not a viable option in our case for the same reason above; each evaluation of the target function

is simply too expensive. For example, for a system with one hundred parameters we would need one hundred and one function evaluations to calculate its gradient.

Luckily, our optimization problem has a lot of structure. Computational experiments come in the form of an average; of these ensemble averages we know a priori the functional form of the probability density. Using this knowledge, it is indeed possible to calculate the full gradient in parameter space as a single ensemble average[13]. The calculation is analytical and affected only by the statistical error associated with the ensemble average.

By direct differentiation we obtain that the gradient vector is[13]:

$$\begin{aligned} \nabla_{\pi}\Theta(\pi) &= 2\sum_{i=1}^{N}\left[\langle O_i\rangle_{\pi} - O_{\exp,i}\right]\nabla_{\pi}\langle O_i\rangle_{\pi} \\ \nabla_{\pi}\langle O_i\rangle_{\pi} &= \langle \nabla_{\pi} O_i\rangle_{\pi} - \beta\left[\langle \nabla_{\pi} H \cdot O_i\rangle_{\pi} - \langle \nabla_{\pi} H\rangle_{\pi}\langle O_i\rangle_{\pi}\right] \end{aligned} \tag{2.4}$$

Where we have used $\nabla_{\pi}\langle O\rangle_{(\pi,T)}$ to denote the sensitivity of the macroscopic observable $\langle O\rangle_{(\pi,T)}$ with respect to the parameters π. The sensitivity measures how much the observable depends on a parameter; if it is zero the observable does not depend on that parameter and no improvement in the target function can be achieved by varying it.

We can also calculate in the same way, as before, any derivative we wish. The Hessian matrix is:

$$\nabla\nabla^T{}_\pi\Theta(\pi) = 2\sum_{i=1}^{N}\left[\langle O_i\rangle_\pi - O_{\exp,i}\right]\nabla\nabla^T{}_\pi\langle O_i\rangle_\pi + 2\sum_{i=1}^{N}\nabla_\pi\langle O_i\rangle_\pi\nabla^T{}_\pi\langle O_i\rangle_\pi$$

$$\begin{aligned}\nabla\nabla^T{}_\pi\langle O\rangle_\pi = &\left\langle\nabla\nabla_\pi{}^T O\right\rangle_\pi \\ &+\beta\left\{\begin{array}{l}-\left\langle\nabla_\pi H\nabla_\pi{}^T O\right\rangle_\pi + \left\langle\nabla_\pi H\right\rangle_\pi\left\langle\nabla_\pi{}^T O\right\rangle_\pi - \left\langle\nabla_\pi O\nabla_\pi{}^T H\right\rangle_\pi - \left\langle O\nabla\nabla_\pi{}^T H\right\rangle_\pi \\ +\left\langle\nabla_\pi O\right\rangle_\pi\left\langle\nabla_\pi{}^T H\right\rangle_\pi + \langle O\rangle_\pi\left\langle\nabla\nabla_\pi{}^T H\right\rangle_\pi\end{array}\right\} \\ &+\beta^2\left\{\begin{array}{l}\left\langle\nabla_\pi H\, O\nabla_\pi{}^T H\right\rangle_\pi - 2\left\langle\nabla_\pi H\right\rangle_\pi\left\langle O\nabla_\pi{}^T H\right\rangle_\pi \\ +2\langle O\rangle_\pi\left\langle\nabla_\pi H\right\rangle_\pi\left\langle\nabla_\pi{}^T H\right\rangle - \langle O\rangle_\pi\left\langle\nabla_\pi H\nabla_\pi{}^T H\right\rangle_\pi\end{array}\right\}\end{aligned} \tag{2.5}$$

Note that the Hessian matrix, while symmetric by construction, is in general indefinite.

Using the information contained in the gradient and the Hessian (calculated for a given parameter set π_0) we can build a quadratic model for the target function $\Theta(\pi)$ in a neighborhood of the point π_0. The quadratic model $m(p)$ is a function of the displacement vector $p = \pi - \pi_0$. The quadratic model is accurate in a neighborhood of π_0; we call this region the Trust Region. We characterize this region of the parameter space by the space contained in a spherical domain of radius Δ. Later on we will explain how the radius can be iteratively updated.

The method we use to solve our optimization problem is called Trust Region Newton (TRNM).[25] We minimize the target function by iteratively updating the parameters set:

$$\pi_{k+1} = \pi_k + p_k \tag{2.6}$$

where the increment p_k is chosen solving the sub-problem:

$$\begin{aligned} p_k &= \arg\min m_k(p) \qquad\qquad \text{s.t. } ||p|| \le \Delta_k \\ m_k(p) &= \Theta(\pi_k) + \nabla^T \Theta(\pi_k)\, p + \frac{1}{2} p^T \nabla\nabla^T \Theta(\pi_k)\, p \end{aligned} \tag{2.7}$$

The sub-problem can be solved in approximated way[25] or exactly; here, given the dimension of the parameter space and having calculated the Hessian, we find the exact solution of the sub-problem following the method of Moré and Sorensen[26] .

TRNM is a very efficient method of local optimization that essentially inherits the same convergence properties of the Newton Method but it is much more stable allowing to deal with indefinite matrices.

The use of the Trust Region restricts the optimization in the surrounding of the point representing the original parameterization; this is a good feature. While one could think that a global minimization is always better than a local one, this is not the case in our application. The current parameters are the result of a great deal of work from many researchers during a few decades; while an improvement may be required it is not advisable to drift too far from the original parameters because other features not under optimization may get worse. We seek the smallest changes in the parameters that do the job; the bigger is the change with respect to the current parameters the smaller is the hope that the new parameters will be transferable to other simulation problems.

Adaptive algorithm for the choice of the Trust Region

The Trust Region is the region in which we consider the quadratic model $m(p)$ to be accurate. There is no way to assess the quality of the model based on one single evaluation of the target function $\Theta(\pi)$ and its derivatives; we can however design an adaptive scheme to update the Trust Region based on the following idea.[25,26]

$m_k(0) - m_k(p_k)$ is the predicted reduction of the target function based on the model; this quantity is always positive. $\Theta(\pi_k) - \Theta(\pi_k + p_k)$ is the actual reduction that we measure after the parameters have been updated; this quantity can be positive or negative. If the actual reduction is negative it means that we did not decrease the value of the target function and therefore the step must be rejected. If instead the actual reduction is positive and its value is similar to the value of the predicted reduction then it means that the model is accurate, at least inside the trust region; in this case we can try to increase the radius of the trust region to make the optimization more efficient. If instead the actual reduction is positive and its value is very different from the predicted reduction then it means that the model is not accurate but we did decrease the value of the target function; in this case we accept the step but we decrease the radius of the Trust Region to find a suitable neighborhood of the current parameter set in which the model is accurate.

We can therefore build an adaptive scheme to update the Trust Region as follows. At iteration k, p_k is the increment to the parameters set and ρ_k is the ratio:

$$\rho_k = \frac{\text{actual reduction}}{\text{predicted reduction}} = \frac{\Theta(\pi_k) - \Theta(\pi_k + p_k)}{m_k(0) - m_k(p_k)} \tag{2.8}$$

The following algorithm prescribes how to iteratively update trust-region radius Δ_k .

Algorithm (*Trust Region*)

Given $\Delta_{\max} > 0, \Delta_0 \in (0, \Delta_{\max})$ and $\eta \in \left[0, \frac{1}{4}\right)$

for $k = 0,1,2,...$

Find p_k *solving the quadratic sub-problem* (2.7)*;*

Evaluate ρ_k *;*

if $\rho_k < \frac{1}{4}$

$$\Delta_{k+1} = \frac{1}{4}\|p_k\|;$$

else

if $\rho_k > \frac{3}{4}$ *and* $\|p_k\| = \Delta_k$

$$\Delta_{k+1} = \min(2\Delta_k, \Delta_{\max});$$

else

$$\Delta_{k+1} = \Delta_k;$$

if $\rho_k > \eta$

$$\pi_{k+1} = \pi_k + p_k;$$

else

$$\pi_{k+1} = \pi_k;$$

end(for)

η is a tuning parameter (kept fixed through the iterations) that is used to optimize the performance of the algorithm; in our case, given the small number of iterations performed, we could not study the efficiency of the algorithm for several values of η. In practice, we used the value $\eta=0$.

Hyper-Elliptical Trust Region

One specific problem of full space optimization of MD force fields lies in the range of values of different parameters; some parameter range of values are in the hundreds of thousands (e.g. some van der Waals parameters), while others are of order one (e.g. torsion coefficients). The difference of several orders of magnitude presents a significant challenge for a stepping minimization algorithm; the resulting optimization is highly inefficient. The step needs to be small enough to follow the steep directions; in this way the step is often so small that the changes in the other directions become negligible. In order to make adjustments that are homogeneous we introduce a scaling matrix D_k such that every element of the vector $\gamma_k = D_k \pi_k$ is of order one. The matrix D_k is a diagonal matrix:

$$\begin{bmatrix} d_1 & & & \\ & d_2 & & \\ & & \ldots & \\ & & & d_n \end{bmatrix}, \qquad d_i = \begin{cases} 1/\left|(\pi_k)_i\right| & \text{if } \left|(\pi_k)_i\right| > 1 \\ 1 & \text{if } \left|(\pi_k)_i\right| \le 1 \end{cases} \tag{2.9}$$

In this way all the parameters are scaled to be in the range -1 to 1.

We can now solve the sub-problem in an elliptical trust region defined by $\left|\left|Dp\right|\right| \le \Delta_k$:

$$
\begin{aligned}
& p_k = \arg\min m_k(p) && \text{s.t. } ||Dp|| \le \Delta_k \\
& m_k(p) = \Theta(\pi_k) + \nabla^T \Theta(\pi_k)\, p + \frac{1}{2} p^T \nabla\nabla^T \Theta(\pi_k)\, p
\end{aligned}
\tag{2.10}
$$

We first cast this elliptical thrust-region problem in the canonical form of an equivalent spherical thrust-region problem in the variable $\gamma_k = D\ p_k$:

$$
\begin{aligned}
& \gamma_k = \arg\min m_k(\gamma) && \text{s.t. } ||\gamma|| \le \Delta_k \\
& m_k(\gamma) = \Theta(\pi_k) + \nabla^T \Theta(\pi_k) D^{-1}\gamma + \frac{1}{2} \gamma^T \left(D^{-1}\right)^T \nabla\nabla^T \Theta(\pi_k) D^{-1}\gamma
\end{aligned}
\tag{2.11}
$$

Then we apply the inverse transformation to obtain $p_k = D^{-1}\gamma_k$.

For a simpler notation, from now on we will define $B = \left(D^{-1}\right)^T \nabla\nabla^T \Theta(\pi_k) D^{-1}$ and $g^T = \nabla^T \Theta(\pi_k) D^{-1}$; we recall that the matrix B is symmetric by construction.

Charge Constraint

The parameters that we optimize include the atomic (partial) charges within a molecule. An obvious constraint on the space of the optimization is the preservation of the molecular charge, i.e. the total molecular charge must not change upon optimization. This is in contrast to other parameters such as bond length. We impose charge conservation as a linear constraint. We write the total charge as $Q = \sum_{l=1}^{m} n_l q_l$ where q_l is the partial charge associated to the atom type l, there are n_l atoms of type l and the total number of atom types is m. Keeping the total charge constant means satisfying the linear constraint $Q_k = Q_0$, where k, as before is the iteration index. Exploiting the linearity of the constraint we can fix the total charge by projecting the increment p_k onto the hyper-plane of constant charge defined by the constraint Q:

$$p_k' = p_k - \frac{p_k \cdot \nabla_\pi Q}{\nabla_\pi Q \cdot \nabla_\pi Q} \nabla_\pi Q \tag{2.12}$$

Solution of the Sub-Problem

We now turn our attention to the sub-problem. If we have N parameters, we are looking for the vector $p \in \mathbb{R}^N$ such that

$$\begin{aligned} p &= \arg\min_{p\in\mathbb{R}^N} m(p) \qquad \text{s.t.} \quad ||p|| \le \Delta \\ m(p) &= f + g^T p + \frac{1}{2} p^T B p \end{aligned} \tag{2.13}$$

where B is a symmetric matrix.

There are many possible approaches to this problem. For example an approximate solution can be found using the Cauchy Point Method, the Dogleg Method or following the Steihaug's approach [25]. Given the dimension of our matrix B it is possible and convenient for us to find a nearly exact solution to the sub-problem. We will follow the method of Moré and Sorensen[25,26].

Let us first prove the following lemma that will be very useful later on in order to characterize the solution of the sub-problem.

Lemma:

Let m be the quadratic function defined by

$$m(p) = f + g^T p + \frac{1}{2} p^T B p$$

where B is any symmetric matrix. Then

(i) *m attains a minimum if and only if B is positive semidefinite and g is in the range of B;*

(ii) *m has a unique minimizer if and only if B is positive definite;*

(iii) *if B is positive semidefinite, then every p satisfying* $Bp = -g$ *is a global minimizer of m.*

Proof.

We prove each of the three statements in turn.

(i) "*if*" part:

Since g is in the range of B there is a p such that $Bp = -g$.

For all $w \in \mathbb{R}^N$ we have

$$\begin{aligned} m(p+w) &= f + g^T(p+w) + \frac{1}{2}(p+w)^T B(p+w) \\ &= f + g^T p + \frac{1}{2} p^T Bp + g^T w + \frac{1}{2} w^T Bw + w^T Bp \\ &= m(p) + g^T w + \frac{1}{2} w^T Bw + (-g)^T w \\ &= m(p) + \frac{1}{2} w^T Bw \\ &\geq m(p) \end{aligned}$$

since B is positive semidefinite. Therefore p is a minimum of m.

(i) "*only if*" part:

Let p be a minimizer of m. Since $\nabla m(p) = Bp + g = 0$, we have that g is in the range of B.

We also have that $\nabla^2 m(p) = B$ is positive semidefinite, giving the result.

(ii) "*if*" part:

Same as in **(i)**, then we note that $\frac{1}{2}w^T Bw > 0$ for all $w \neq 0$

(ii) *"only if"* part:

Same as in **(i)** to prove that B is positive semidefinite. If B is not positive definite then there is a vector $w \neq 0$ such that $\frac{1}{2}w^T Bw = 0$. Hence $m(p+w) = m(p)$ and the minimizer is not unique, giving contradiction.

(iii) Follows from the proof of **(i)**.

To see that, consider the matrix B

$$B = \begin{bmatrix} 1 & 0 & 0 \\ 0 & 0 & 0 \\ 0 & 0 & 5 \end{bmatrix}$$

which is singular and it has eigenvalues 0, 1, 5. If g is any vector whose second component is zero then g in the range of B. In this case the quadratic function attains a minimum. If instead the second component of g is non-zero, we can indefinitely decrease $m(\cdot)$ by moving along the direction $(0,-g_2,0)$.

Using the lemma above we can now state and prove the following theorem that gives a precise characterization of the solution of spherical thrust-region problem.

Theorem:

The vector $p^* \in \mathbb{R}^N$ *is a global solution of the trust-region problem*

$$\min_{p\in\mathbb{R}^N} m(p) = f + g^T p + \frac{1}{2} p^T B p, \qquad \text{s.t.} \quad ||p|| \le \Delta \tag{2.14}$$

if and only if $||p^*|| \le \Delta$ *and there is a scalar* $\lambda \ge 0$ *such that the following conditions are satisfied:*

$$\begin{aligned} &(B + \lambda I) p^* = -g \\ &\lambda\left(\Delta - ||p^*||\right) = 0 \\ &(B + \lambda I) \quad \text{is positive semidefinite} \end{aligned} \tag{2.15}$$

Proof.

"if" part:

Assume there exists a $\lambda \ge 0$ such that the conditions (2.15) are satisfied. (iii) of the preliminary lemma guarantees that p^* is a global minimum of the quadratic function:

$$\hat{m}(p) = f + g^T p + \frac{1}{2} p^T (B + \lambda I) p = m(p) + \frac{\lambda}{2} p^T p$$

Since $\hat{m}(p) \geq \hat{m}(p^*)$ we have:

$$m(p) \geq m(p^*) + \frac{\lambda}{2}\left((p^*)^T p^* - p^T p\right)$$

Since $\lambda\left(\Delta - \|p^*\|\right) = 0$ then we have $\lambda\left(\Delta^2 - (p^*)^T p^*\right) = 0$. We can therefore substitute this relation into the formula above to obtain:

$$m(p) \geq m(p^*) + \frac{\lambda}{2}\left(\Delta^2 - p^T p\right)$$

So for every $\lambda \geq 0$ we have $m(p) \geq m(p^*)$ for all $\|p\| \leq \Delta$. Therefore, p^* is the solution of (2.14)

"only if" part:

Let us now assume that p^* is the solution of (2.14) and show that there is a $\lambda \geq 0$ that satisfies (2.15).

In the case $\|p^*\| < \Delta$, p^* is the unconstrained minimizer of *m(p)*. Therefore $\nabla m(p^*) = Bp^* + g = 0$ and $\nabla^2 m(p) = B$ is positive semidefinite. For $\lambda = 0$ all the conditions are verified.

From now on we will deal exclusively with the case $\|p^*\| = \Delta$. The second condition of (2.15) is immediately verified. p^* solves the constrained problem

$$\min_{p\in\mathbb{R}^N} m(p) = f + g^T p + \frac{1}{2} p^T B p, \qquad \text{s.t.} \quad ||p|| = \Delta$$

We can apply Lagrange Multipliers to obtain the Lagrangian:

$$L(p,\lambda) = m(p) + \frac{\lambda}{2}\left(p^T p - \Delta^2\right)$$

We then find the stationary point p^* such that $\nabla_p L\left(p^*,\lambda\right) = 0$:

$$Bp^* + g + \lambda p^* = 0 \;\Rightarrow\; \left(B + \lambda I\right) p^* = -g$$

So we have proved that the first condition of (2.15) holds.

To prove the last condition we use the fact that $m(p) \geq m(p^*)$ for any p such that $p^T p = \left(p^*\right)^T p^* = \Delta^2$. Therefore we have:

$$m(p) \geq m(p^*) + \frac{\lambda}{2}\left(\left(p^*\right)^T p^* - p^T p\right)$$

We can now substitute in $\left(B + \lambda I\right) p^* = -g$ and rearrange the terms to obtain:

$$\frac{1}{2}\left(p - p^*\right)^T \left(B + \lambda I\right)\left(p - p^*\right) \geq 0$$

Since the set of directions

$$\left\{ w : w = \pm \frac{p - p^*}{\left|\left| p - p^* \right|\right|} \text{ for some } \left|\left| p \right|\right| = \Delta \right\}$$

is dense on the unit sphere then the third condition (2.15) is proved.

It only remains to show that λ is positive. Since $(B + \lambda I)p^* = -g$ and $B + \lambda I$ is positive definite we know from (i) of the preliminary lemma that p^* is the global minimizer of $\hat{m}(p)$ and therefore:

$$m(p) \geq m(p^*) + \frac{\lambda}{2}\left((p^*)^T p^* - p^T p \right)$$

Assume now that only $\lambda < 0$ can satisfy the conditions (2.15), we have:

$$m(p) \geq m(p^*) \text{ for every } \left|\left| p \right|\right| \geq \left|\left| p^* \right|\right| = \Delta$$

We now recall that at the beginning of the proof we assumed that p^* minimizes $m(p)$ for $\left|\left| p \right|\right| \leq \Delta$; p^* is therefore the unconstrained minimizer of $m(p)$.

If p^* is therefore the unconstrained minimizer of $m(p)$ by the preliminary lemma we have that B is positive semidefinite and $Bp^* = -g$; as a consequence, $\lambda = 0$ verifies the conditions (2.15) contradicting our assumption. We conclude that $\lambda \geq 0$ completing the proof.

The theorem that we have just proved enables us to write an algorithm to find the solution of the sub-problem. If B is positive definite and $\left\|p^*\right\| \le \Delta$ then $\lambda = 0$ and we have our solution; otherwise we look for a solution of the form:

$$\begin{aligned} p(\lambda) &= -(B+\lambda I)^{-1} g = -Q(\Lambda+\lambda I)^{-1} Q^T g \\ &= -\sum_{j=1}^{n} \frac{q_j{}^T g}{\lambda_j + \lambda} q_j \end{aligned} \tag{2.16}$$

where we have used the fact that $(B+\lambda I)$ is a real symmetric matrix and therefore Q is an orthogonal matrix.

We now look for the Lagrange Multiplier $\lambda \in (-\lambda_1, \infty)$ that is the solution of the equation

$$\phi_1(\lambda) = \left\|p(\lambda)\right\| - \Delta = 0 \tag{2.17}$$

The above equation is highly nonlinear in λ when λ is close to $-\lambda_1$; in this case it would be very difficult to find the desired solution of the equation. To remedy this problem we solve the following equivalent equation that has the advantage of being nearly linear for λ close to $-\lambda_1$:

$$\phi_2(\lambda) = \frac{1}{\Delta} - \frac{1}{||p(\lambda)||} = 0 \tag{2.18}$$

To solve (2.18) we use the standard Newton's Iteration:

$$\lambda^{(l+1)} = \lambda^{(l)} - \frac{\phi_2\left(\lambda^{(l)}\right)}{\phi'_2\left(\lambda^{(l)}\right)} \tag{2.19}$$

A practical implementation of the iteration above is the following:

Algorithm (*Exact Trust Region*)

Given $\lambda^{(0)}, \Delta > 0$

for $l = 0,1,2,...$

Factor $B + \lambda^{(l)} I = R^T R$

Solve $R^T R p_l = -g, \;\; R^T q_l = p_l$

Set $\lambda^{(l+1)} = \lambda^{(l)} + \left(\frac{||p_l||}{||q_l||}\right)^2 \left(\frac{||p_l|| - \Delta}{\Delta}\right)$

end(for)

To write the algorithm we have used the Cholesky factorization $B+\lambda I = R^T R$ and we have used the following definition:

$$\begin{aligned} \|q\|^2 &= \left\|R^{-T} p\right\|^2 = p^T \left(B+\lambda I\ \right)^{-1} p \\ &= g^T Q(\Lambda+\lambda I)^{-1} Q^T Q(\Lambda+\lambda I)^{-1} Q^T Q(\Lambda+\lambda I)^{-1} Q^T g \\ &= g^T Q(\Lambda+\lambda I)^{-3} Q^T g = -\sum_{j=1}^{n} \frac{\left\|q_j{}^T g\right\|^2}{\left(\lambda_j+\lambda\right)^3} \end{aligned} \tag{2.20}$$

and we therefore have:

$$\begin{aligned} \phi_2{}'(\lambda) &= \frac{d}{d\lambda}\left(\|p(\lambda)\|^2\right)^{-\frac{1}{2}} = -\frac{1}{2}\left(\|p(\lambda)\|^2\right)^{-\frac{3}{2}} \frac{d}{d\lambda}\left(\|p(\lambda)\|^2\right) \\ &= \frac{1}{\|p(\lambda)\|^3} \sum_{j=1}^{n} \frac{\left(q_j{}^T g\right)^2}{\left(\lambda_j+\lambda\right)^3} = \frac{1}{\|p\|^3}\|q\|^2 \end{aligned} \tag{2.21}$$

The initial $\lambda^{(0)}$ is set to be zero if the matrix B is positive definite. If the matrix B is indefinite is instead set to be $\lambda^{(0)} = -\min\left\{\lambda_1^-, \lambda_2^-, ...,\right\} + 0.00001$ where $\left\{\lambda_1^-, \lambda_2^-, ...,\right\}$ are the negative eigenvalues of the matrix B. In this way that $B+\lambda^{(0)} I$ is always positive definite, and it is therefore possible to perform its Cholesky Factorization.[27]

Use of POP in conjunction with other common computational techniques

The calculation of thermodynamic and kinetic properties of condensed phase systems is a very challenging computational problem; typically, the model has tens of thousands degrees of freedom and the time required to reach sufficient sampling is in the order of microseconds while the time step used is 1 or 2 femtoseconds. We therefore have to apply our time-stepping algorithm $\sim 10^9$ times; the final time required for the computation adds up to tens of thousands of CPU hours for each iteration of the minimization algorithm.

Parallelization of the MD engine helps in reducing the time required to collect statistics but it is not sufficient; the use of enhanced sampling techniques to accelerate convergence of the averages is in many cases of vital importance.

In this section we will review two of the most common enhanced sampling techniques (Umbrella Sampling and Replica Exchange Molecular Dynamics) used in condensed phase simulations and we will see how they can work in conjunction with the POP method.

We will also see how POP can be combined with Thermodynamic Integration[28] (TI) in order to use as experimental target measurements of free energy. This is an important addition to the method given the availability of free energy measurements in literature.

Replica Exchange Molecular Dynamics

REMD [29,30] is efficient, intrinsically parallel and is the method of choice to study the temperature dependence of an *in silico* measurement.

REMD constructs the probability distribution of an extended ensemble consisting of N non-interacting replicas of the original system in the canonical ensemble at N different temperatures T_i. The weight associated with a certain state x_i belonging to replica i is:

$$w(x_i) = e^{-\beta_i U(x_i)} \tag{2.22}$$

where $\beta_i = \frac{1}{kT_i}$. As already shown, in our case for each replica this probability distribution is obtained through MD.

The weight distribution of the extended ensemble is thus:

$$W_{REMD}(X) = e^{-\sum_i \beta_i U(x_i)} \tag{2.23}$$

with $X = (x_1, x_2, x_3, ..., x_N)$.

A Metropolis Monte Carlo Markov Chain (MCMC) algorithm randomly selects two trajectories and swaps the coordinates of the two trajectories according to a Boltzmann -like weight:

$$p_{x_i \to x_j} = \min\left(1, e^{-(\beta_i - \beta_j)(U(x_j) - U(x_i))}\right) \tag{2.24}$$

Detailed balance is verified and so the existence of the equilibrium distribution W_{REMD}:

$$W_{REMD} p_{x_i \to x_j} = W_{REMD} p_{x_j \to x_i} \tag{2.25}$$

The result of this procedure is that each trajectory, while exploring the equilibrium distribution at each single temperature, is a random walker in the temperature domain. Structures sampled from high-temperature trajectories are made available to the low-temperature trajectories allowing rapid exchanges between metastable states and thus improving the convergence of thermodynamics observable at the more interesting lower temperatures.

Moreover, if we are interested in the observable as a function of the temperature (as it often happens) the enhancement of the sampling comes at no cost. In our implementation the integration of the trajectory of each one of the replicas is parallelized over multiple cores in the same node.

Umbrella sampling

Umbrella sampling [31] is a computational technique used to improve sampling when ergodicity is hindered by the shape of the energy landscape. It is a method closely related to importance sampling in statistics.

Systems with an energy barrier separating two regions of the configuration space may suffer from poor sampling, as the time required to cross the barrier is exponentially long with the height of the barrier. Umbrella sampling is a method that overcomes this problem introducing a biasing potential V .

$$\langle O \rangle_H = \frac{\langle O e^{\beta V} \rangle_{H+V}}{\langle e^{\beta V} \rangle_{H+V}} \tag{2.26}$$

Using the biasing potential it is possible to constrain the system to a certain region and collect sufficient sampling for that region; subsequently, it is possible to combine the sampling obtained with different biasing potentials to reconstruct the complete free energy landscape [31].

The biasing potential is usually introduced by the use of a reaction coordinate $q(x)$, i.e. a mapping from the coordinate space to a space of reduced dimensionality (most often q is a scalar). The ensemble average of an observable O that depends explicitly on q can be rewritten as:

$$\langle O \rangle_H = \int O(q^*, \pi) f_\pi(q^*) dq^*$$
$$f_\pi(q^*) = \frac{\int e^{-\beta H(x,p,\pi)} \delta(q(x) - q^*) dx\, dp}{\int e^{-\beta H(x,p,\pi)} dx\, dp} \tag{2.27}$$

We can now apply the biasing potentials as a function of the reaction coordinate; for example we use a harmonic potentials $V_i(x) = \gamma(q(x) - q_i)^2$, obtaining:

$$f_\pi(q^*) = \frac{\int e^{-\beta H(x,p,\pi)} e^{-\beta V_i} e^{+\beta V_i} \delta(q(x) - q^*) dx dp}{\int e^{-\beta H(x,p,\pi)} dx dp}$$
$$= \frac{\left\langle e^{+\beta V_i} \delta(q(x) - q^*) \right\rangle_{H+V_i}}{\left\langle e^{+\beta V_i} \right\rangle_{H+V_i}} = \frac{e^{+\beta V_i(q^*)} \left\langle \delta(q(x) - q^*) \right\rangle_{H+V_i}}{\left\langle e^{+\beta V_i} \right\rangle_{H+V_i}} \tag{2.28}$$

The denominator $\left\langle e^{+\beta V_i} \right\rangle_{H+V_i}$ is a constant that cannot be calculated from the sampling; instead, using two different biasing potentials V_{i+1} and V_i we can calculate the following ratio:

$$\frac{\left\langle e^{+\beta V_{i+1}} \right\rangle_{H+V_{i+1}}}{\left\langle e^{+\beta V_i} \right\rangle_{H+V_i}} = \frac{e^{+\beta V_{i+1}(q^*)} \left\langle \delta(q(x) - q^*) \right\rangle_{H+V_{i+1}}}{e^{+\beta V_i(q^*)} \left\langle \delta(q(x) - q^*) \right\rangle_{H+V_i}} \tag{2.29}$$

We are therefore able to determine $f_\pi(q^*)$ only up to an unknown multiplicative constant. This is enough information if (as often happens in the study of chemical reactions) all we are interested in is the relative probability of two regions of the phase space. In this case we can use POP proceeding as it follows. First, let us divide the phase space in two regions A and B. We have the probabilities:

$$\begin{aligned} P(A) &= \int_{q^* \in q(A)} f_\pi(q^*)\,dq^* = \int_{q^* \in q(A)} \frac{\int e^{-\beta H(x,p,\pi)} \delta(q(x) - q^*)\,dx dp}{\int e^{-\beta H(x,p,\pi)}\,dx dp}\,dq^* \\ &= \frac{1}{Z}\int_{q^* \in q(A)} \int e^{-\beta H(x,p,\pi)} \delta(q(x) - q^*)\,dx\,dp\;dq^* \\ P(B) &= \int_{q^* \in q(B)} f_\pi(q^*)\,dq^* = \int_{q^* \in q(B)} \frac{\int e^{-\beta H(x,p,\pi)} \delta(q(x) - q^*)\,dx dp}{\int e^{-\beta H(x,p,\pi)}\,dx dp}\,dq^* \\ &= \frac{1}{Z}\int_{q^* \in q(B)} \int e^{-\beta H(x,p,\pi)} \delta(q(x) - q^*)\,dx\,dp\;dq^* \end{aligned} \tag{2.30}$$

where we have used the partition function $Z = \int e^{-\beta H(x,p,\pi)}\,dx dp$.

It is possible to optimize the parameters using the ratio of probabilities $\frac{P(A)}{P(B)}$ as a target:

$$\begin{aligned}\nabla_\pi \frac{P(A)}{P(B)} &= \nabla_\pi \frac{\frac{1}{Z}\int_{q^*\in q(A)}\int e^{-\beta H(x,p,\pi)}\delta\left(q(x)-q^*\right)dx\,dp\;dq^*}{\frac{1}{Z}\int_{q^*\in q(B)}\int e^{-\beta H(x,p,\pi)}\delta\left(q(x)-q^*\right)dx\,dp\;dq^*} \\ &= -\beta\frac{\int_{q^*\in q(A)}\int e^{-\beta H(x,p,\pi)}\nabla_\pi H\;\delta\left(q(x)-q^*\right)dx\,dp\;dq^*}{\int_{q^*\in q(B)}\int e^{-\beta H(x,p,\pi)}\delta\left(q(x)-q^*\right)dx\,dp\;dq^*} \\ &+\beta\frac{\int_{q^*\in q(A)}\int e^{-\beta H(x,p,\pi)}\delta\left(q(x)-q^*\right)dx\,dp\;dq^*}{\int_{q^*\in q(B)}\int e^{-\beta H(x,p,\pi)}\delta\left(q(x)-q^*\right)dx\,dp\;dq^*}\bullet \\ &\bullet\frac{\int_{q^*\in q(B)}\int e^{-\beta H(x,p,\pi)}\nabla_\pi H\;\delta\left(q(x)-q^*\right)dx\,dp\;dq^*}{\int_{q^*\in q(B)}\int e^{-\beta H(x,p,\pi)}\delta\left(q(x)-q^*\right)dx\,dp\;dq^*}\end{aligned} \tag{2.31}$$

Each one of the averages above can be computed as we did in (2.28):

$$\begin{aligned}\frac{\int e^{-\beta H(x,p,\pi)}\delta\left(q(x)-q^*\right)dxdp}{\int e^{-\beta H(x,p,\pi)}dxdp} &= \frac{e^{+\beta V_i\left(q^*\right)}\left\langle\delta\left(q(x)-q^*\right)\right\rangle_{H+V_i}}{\left\langle e^{+\beta V_i}\right\rangle_{H+V_i}} \\ \frac{\int e^{-\beta H(x,p,\pi)}\nabla_\pi H\;\delta\left(q(x)-q^*\right)dxdp}{\int e^{-\beta H(x,p,\pi)}dxdp} &= \frac{e^{+\beta V_i\left(q^*\right)}\left\langle\nabla_\pi H\;\delta\left(q(x)-q^*\right)\right\rangle_{H+V_i}}{\left\langle e^{+\beta V_i}\right\rangle_{H+V_i}}\end{aligned} \tag{2.32}$$

As before, each one of the averages above is known up to a multiplicative constant that is the same for every term. The unknown constant cancels in (2.31) allowing us to calculate the unbiased sensitivity of the ratio $\frac{P(A)}{P(B)}$.

Thermodynamic Integration

Thermodynamic integration (TI)[28] is a method used to compare the difference in free energy between two given states (e.g. A and B) . In the TI approach the free energy difference is calculated by integrating over free energy changes along a path connecting the two states. Such a path can be a real chemical process or an alchemical process.

Consider the Hamiltonian:

$$H(x,p,\pi,\lambda)=\sum_i \frac{p_i^2}{2m_i}+U_A(\pi,x)+\lambda\left(U_B(\pi,x)-U_A(\pi,x)\right) \tag{2.33}$$

$H(\lambda)$ parametrically depends on λ; for $\lambda=0$ represents the Hamiltonian of state A while for $\lambda=1$ represents the Hamiltonian of state B.

The free energy also is a function of λ:

$$F(\pi,\lambda)=-\frac{1}{\beta}\ln\int e^{-\beta H(x,p,\pi,\lambda)}dxdp \tag{2.34}$$

We can therefore calculate the difference in free energy between the state A and the state B as:

$$\begin{aligned}\Delta F(A \to B;\pi) &= \int_0^1 d\lambda \frac{dF(\pi,\lambda)}{d\lambda} = \int_0^1 d\lambda \frac{\int e^{-\beta H(x,p,\pi,\lambda)} \frac{dH(x,p,\pi,\lambda)}{d\lambda} dxdp}{\int e^{-\beta H(x,p,\pi,\lambda)} dxdp} \\ &= \int_0^1 d\lambda \left\langle U_B(\pi,x) - U_A(\pi,x) \right\rangle_{(\pi,\lambda)}\end{aligned} \tag{2.35}$$

Any target function $\Theta(\pi)$ depending on ΔF_π can therefore be minimized using POP:

$$\begin{aligned}\nabla_\pi \Theta(\pi) &= \frac{d\Theta}{d\Delta F} \nabla_\pi \Delta F \\ \nabla_\pi \Delta F &= \int_0^1 d\lambda \nabla_\pi \left\langle U_B - U_A \right\rangle_{(\pi,\lambda)} \\ &= \int_0^1 d\lambda \left\langle \nabla_\pi \left(U_B - U_A \right) \right\rangle_{(\pi,\lambda)} \\ &\quad -\beta \int_0^1 d\lambda \left[\left\langle \nabla_\pi H \cdot \left(U_B - U_A \right) \right\rangle_{(\pi,\lambda)} - \left\langle \nabla_\pi H \right\rangle_{(\pi,\lambda)} \left\langle \left(U_B - U_A \right) \right\rangle_{(\pi,\lambda)} \right]\end{aligned} \tag{2.36}$$

POP applied to structural properties of peptides[c]

In this chapter we focus on conformational transitions and folding of small peptides. We illustrate that the current functional form of the potential energy is sufficiently flexible so that force field parameters can be found that reproduce the folding fraction at room temperature. In fact the folding fraction is an extremely sensitive function of the torsion parameters, so it is not obvious that a particular set of parameters that we fit for one peptide will be transferrable to other folding problems.

We also demonstrate that peptide potential energy parameters that reproduce their melting curves are much harder to identify. We conjecture, based on our numerical optimization, that no peptide potential parameters could be found that reproduce the correct melting curve of peptide folding with the current functional form of the energy.

These observations illustrate the usefulness of the POP approach that not only provides a suitable set of parameters for a particular case but also examine the feasibility and sensitivity of the fitting process.

We stress that our aim is not to produce a general force field for proteins or peptides; here we are exclusively investigating the properties of the current functional form of MD force fields and the existence of a parameterization able to reproduce the

---

[c] Part of the content of this chapter was previously published in collaboration with Ron Elber in

Di Pierro and Elber (2013). "*Automated Optimization of Potential Parameters*."
J. Chem. Theory Comput., **2013**, *9* (8), pp 3311–3320, **DOI:** 10.1021/ct400313n

Ron Elber supervised the work.

temperature dependence of the folded fraction as observed in experiments. In this case we are not concerned about transferability; if we were instead developing a force field for general use then transferability would be an important issue and we would need to show how parameters the fits well the behavior of the molecule used for optimization are also good in fitting the behavior of other molecules. When necessary, the problem of transferability has an obvious but laborious solution: to fit many different observables over many different molecules. In that case we would use a target function of the type:

$$\Theta(\pi) = \sum_{i \in \text{observables}} \sum_{j \in \text{molecules}} \left(\left\langle O_{(i,j)} \right\rangle_{(\pi,N,V,T)} - O^{\exp}{}_{(i,j)} \right)^2 \tag{3.1}$$

The results presented in this chapter are obtained by the use of the sensitivity vector but precede the introduction of the Newton Trust Region in POP. The algorithm used was Steepest Descent. Modifying the set of parameters along the direction of the gradient guarantees maximum change in the value of the target function with a minimum displacement of the parameter values. Steepest Descent minimization is the simplest optimization algorithm, and operates following the recipe:

$$\Delta\pi_i = \pi_{i+1} - \pi_i = -\alpha_i \nabla_\pi \Theta(\pi_i) \tag{3.2}$$

where α is a scalar parameter. We estimate the parameter α by use of the following

heuristic method. First, we calculate the expected change in the target function $\Theta(\pi)$ for a displacement $\Delta\pi$ in the linear regime:

$$\Delta\Theta(\pi_i) \simeq \nabla_\pi \Theta(\pi_i) \cdot \Delta\pi_i = -\alpha_i \nabla_\pi \Theta(\pi_i) \cdot \nabla_\pi \Theta(\pi_i) \tag{3.3}$$

Then, we pick the desired change Δ_i^* for the function $\Theta(\pi)$; finally, we choose α such that:

$$\Delta_i{}^* = -\alpha_i \nabla_\pi \Theta(\pi_i) \cdot \nabla_\pi \Theta(\pi_i) \tag{3.4}$$

Deciding the optimal value of Δ_i^* is not obvious and it varies from case to case; in our first illustration, shifting the conformational equilibrium of alanine dipeptide, we choose $\Delta_i^* = -\Theta(\pi_i)$. This is the maximal change we can have (the minimum of the target function is at zero). This is a large step. However, the torsion potentials, that make the largest contribution to the alanine dipeptide problem, are linear in their parameters (note that the thermodynamic average is not linear). Therefore the regression expression is approximately quadratic which is appropriate for large Newton-Raphson-like steps. In this case the minimization is equivalent to the Newton-Raphson algorithm to find roots of a real valued function

$$\alpha_i = \frac{\Theta(\pi_i)}{\nabla_\pi \Theta(\pi_i) \cdot \nabla_\pi \Theta(\pi_i)},$$
$$\pi_{i+1} = \pi_i - \frac{\Theta(\pi_i) \nabla_\pi \Theta(\pi_i)}{\nabla_\pi \Theta(\pi_i) \cdot \nabla_\pi \Theta(\pi_i)} \tag{3.5}$$

In our second application of optimizing the potential for a pentapeptide, the system deviates significantly from the quadratic description and we used progressively smaller Δ_i^* with the smallest value being just 1% of the $\Theta(\pi_i)$.

This first version of the POP algorithm consists on iterating the following steps:

1 *Compute* $\Theta(\pi_i)$ *and* $\nabla_\pi \Theta(\pi_i)$ *by MD simulations. If* $\Theta(\pi_i)$ *is lower than a threshold* ε *then stop. Otherwise continue to 2.*

2 *Compute* α_i

3 *Compute the new parameters* π_{i+1}

4 *Compute* $\Theta(\pi_{i+1})$.

If $\Theta(\pi_{i+1}) < \Theta(\pi_i)$ *accept the new parameters. Go to 1*

If $\Theta(\pi_{i+1}) \geq \Theta(\pi_i)$ *reject the new parameters, reduce* α_i *and Go to 3*

Alanine dipeptide

Solvated alanine dipeptide has been a model system in computational molecular biophysics for a long time. Here we examine it as a toy model for which the answer can be easily guessed. Our aim it to test if the algorithm POP is able to effectively modify the folded fraction of peptides. We obtain the optimal potential using our automated POP procedure.

Experimental setup

We consider the "toy problem" of solvated alanine dipeptide that was simulated as follows. The program used for Molecular Dynamics simulations was MOIL [15]. The initial force field parameters were the united atom version of OPLS [32] (the covalent parameters are from AMBER [33]). The water model was TIP3P [23]. The blocked alanine dipeptide was solvated in a periodic box of $19.6^3 Å^3$ with 248 water molecules. The simulations were conducted at constant temperature of 300K (NVT ensemble) using velocity scaling. The equations of motion were integrated with a RESPA algorithm [34] employing two time steps (1fs and 4fs). Water molecules were matrix SHAKED [35] with allowed relative errors in bond lengths of 10^{-12}. SHAKE [36] was introduced on the peptide bonds involving hydrogen atoms with tolerance 10^{-12} Å. The time step was 1 fs. The Lennard Jones interactions were truncated as at 8.5 Å using a buffer cutoff of 1 Å. Electrostatic interactions were computed with Particle Mesh Ewald [37] that was used with

error tolerance of 10^{-9} in reciprocal space and grid 20x20x20. For each of the iterations of parameter optimization 100ns of a MD simulation was run to compute the sensitivity. A structure was save each 1ps, thus providing a total of 100,000 structures that were processed by the program POP to calculate the observable and its gradient and optimize the potential parameters as described in Table 1.

Results

The conformational state of alanine dipeptide can be characterized by two soft degrees of freedom, the dihedral angles (φ,ψ).

Figure 1 shows the probability density of configurations as a function of (φ,ψ) calculated with the united atom OPLS [32]: all the populated states are located in the region with negative φ (quadrants II and III). The region with highest probability density is in quadrant III and it corresponds to helical states.

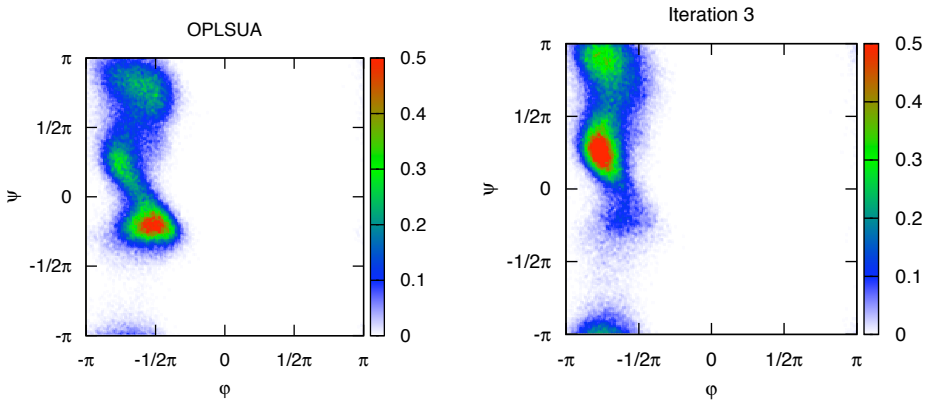

Figure 1: Evolution of the probability density of the dihedral angles (φ,ψ) for alanine dipeptide. The graph on the left shows results obtained with the force field OPLS with united atoms; a propensity to be in helix configuration is indicated by the high-density region in quadrant III. The optimization process reduces the amount of structures in the helical configuration (quadrant III) to the prescribed value (right).

We define our microscopic observable $O(x,p)$ to be the following indicator function:

$$I(\psi) = \begin{matrix} 1 & -100^\circ \le \psi \le 0^\circ \\ 0 & elsewhere \end{matrix} \tag{3.6}$$

The ensemble average of the function $I(\psi)$ is the probability of finding the molecule in the defined region. At 300K approximately 38% of the structures analyzed have ψ -angle that falls in the range -100° to 0°, therefore:

$$\langle I \rangle_{(OPLSUA,300K)} = 0.38 \tag{3.7}$$

As a proof of principle, we use POP to modify the energy parameters to make the helix region unfavorable. This change does not imply (of course) that the preferred conformation of alanine dipeptide in nature is of extended chain. Nevertheless, it is a useful exercise to illustrate the POP algorithm. We seek to modify the force field in such a way that exactly 10% of the structures lie in the helical region, therefore for the function $I(\psi)$ we set up a target value $I_{TARGET} = 0.1$. We will use a single temperature, so the distance function that we use is:

$$\Theta(\pi) = \left(\langle I \rangle_{(\pi,300K)} - I_{TARGET} \right)^2 \tag{3.8}$$

We minimized $\Theta(\pi)$ as a function of the parameters of the proper torsions and Lennard-Jones interactions. These energy terms are typical targets for optimization. Charges are frequently determined by quantum mechanic calculations and we have them fixed in the present manuscript. The total number of parameters that we consider is 72.

One iteration reduces the target function significantly; after three iterations the $\Theta(\pi)$ distance function is $2 \text{x} 10^{-5}$ where $\langle I \rangle_{(POP,300K)} = 0.106 \pm 0.005$ and the target was considered achieved (Figure 2).

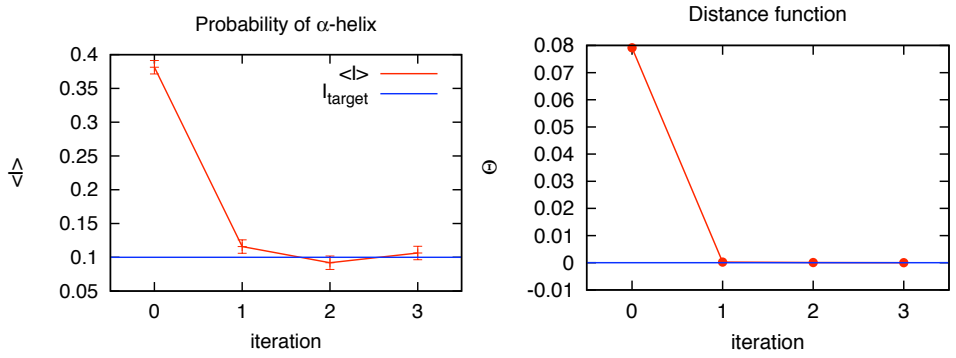

Figure 2: Left: Evolution of probability of α-helical configuration as a function of the iteration number. The target value is achieved in 3 iterations. Right: The distance function $\Theta(\pi)$ as a function of the iteration number.

Figure 3 shows the difference in the dynamics of a trajectory obtained with united atom OPLS and one obtained with the last version of the modified potential. When simulated with the original force field the molecule has frequent transitions between the helical state and the extended chain state spending a significant amount of time in the helical state; when simulated with the modified potential the molecule undergoes fewer transitions into the helical state and the amount of time spent in that state is reduced to the one prescribed as a target.

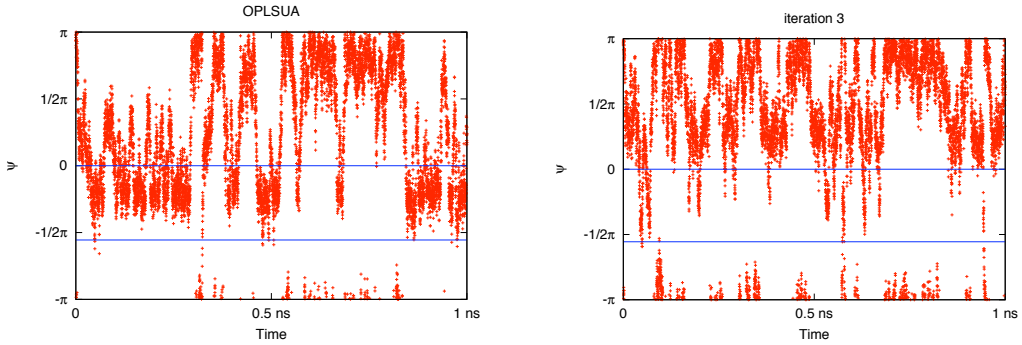

Figure 3: A comparison between a trajectory obtained with the force field OPLSUA (top) and a trajectory obtained with the last iteration of the modified force field (bottom). Both the trajectories are 1ns long. The original force field shows frequent transition in and out of the helical state whose boundaries (as we defined them) are indicated in blue. The molecule spends ~38% of the time in the helical configuration. The modified force field in the bottom figure shows fewer transitions to the helical state where the molecule spends ~10% of the time.

To explore variations in the target function we repeated the POP optimization using a different target; this time instead of reducing the probability of the helical state we increase the probability of the extended chain state. We defined the extended chain state by a range of the ψ-angle (between 90° and 180°); and set $I_{TARGET} = 0.9$. The results are shown in Figure 4, the target was essentially achieved with just one optimization step.

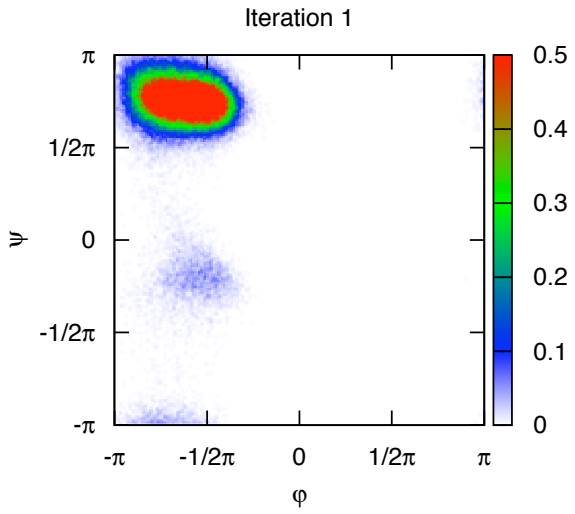

Figure 4: The probability density of states for alanine dipeptide. In this second test we increased the target probability of extended chain to 0.9.

The probability of helix as well as the probability of β-sheet is largely determined by the torsion potential; the sensitivity with respect to the Lennard-Jones parameters is very small and little to no change was made to those parameters.

In MOIL, all possible torsions are generated based on the bond structure that is computed from the system sequence and prior database of amino acid connectivity. In a second step these torsions are assigned values according to the force field at hand. Torsions that do not have contributions to the energy are removed from the list to save computational resources. However, during the optimization it is important to consider also torsions that have no contributions to the current force field but may have one in a refined force field. The POP code was therefore modified to take into account torsion terms with zero coefficients and to compute their parameter derivatives.

Alanine dipeptide has 16 torsions subdivided into 13 torsion types (a torsion type is defined by all four types of atoms in sequence, either in the forward or backward directions). Of the 13 torsion types, 5 torsions are initially set as having no contribution to the energy. Perhaps not surprisingly most of the changes in the force field following POP are in those torsions. POP procedure returns more non-zero torsion coefficients. The stiff torsions (rotations of the amide planes) remain stiff as they should and the free torsions remain relatively soft, even if the coefficients are no longer zero. It is striking that the small, distributed changes of the force field have dramatic effects on the general behavior of the molecule as demonstrated by the density plots.

Torsion Type		Starting parameters			POP	
	a_1	a_2	a_3	a_1	a_2	a_3
43	0.0000	2.5000	0.0000	-0.0001	2.4998	-0.0005
47	0.0000	2.5000	0.0000	0.0000	2.4999	0.0002
45	0.0000	2.5000	0.0000	0.0000	2.4999	0.0004
51	0.0000	2.5000	0.0000	0.0000	2.4999	-0.0003
17	0.0000	0.0000	0.0000	0.0586	-0.1096	0.0305
76	0.0000	0.0000	0.0000	-0.0682	0.0873	0.0434
30	0.0000	0.0000	0.0000	-0.0604	-0.1110	-0.0289
79	0.0000	0.0000	0.0000	0.0704	0.0883	-0.0408
64	0.0000	0.0000	0.1000	0.2167	-0.0354	0.0375
140	0.0000	0.0000	0.0000	-0.2157	0.2981	0.0548
60	0.0000	2.5000	0.0000	0.0000	2.4999	-0.0002
56	0.0000	2.5000	0.0000	0.0000	2.5001	-0.0002
55	0.0000	2.5000	0.0000	0.0000	2.4999	0.0005

Table 1: Coefficients in the expansion of a torsion energy term α $U_\alpha(\phi) = \sum_n a_{n,\alpha}\left[1+\cos\left(n\cdot\phi-\delta_{n,\alpha}\right)\right]$. Only the coefficients a_n are optimized. δ_n is fixed at π. Sample of torsion types, their atom types, and their corresponding indices are shown in Figure 5.

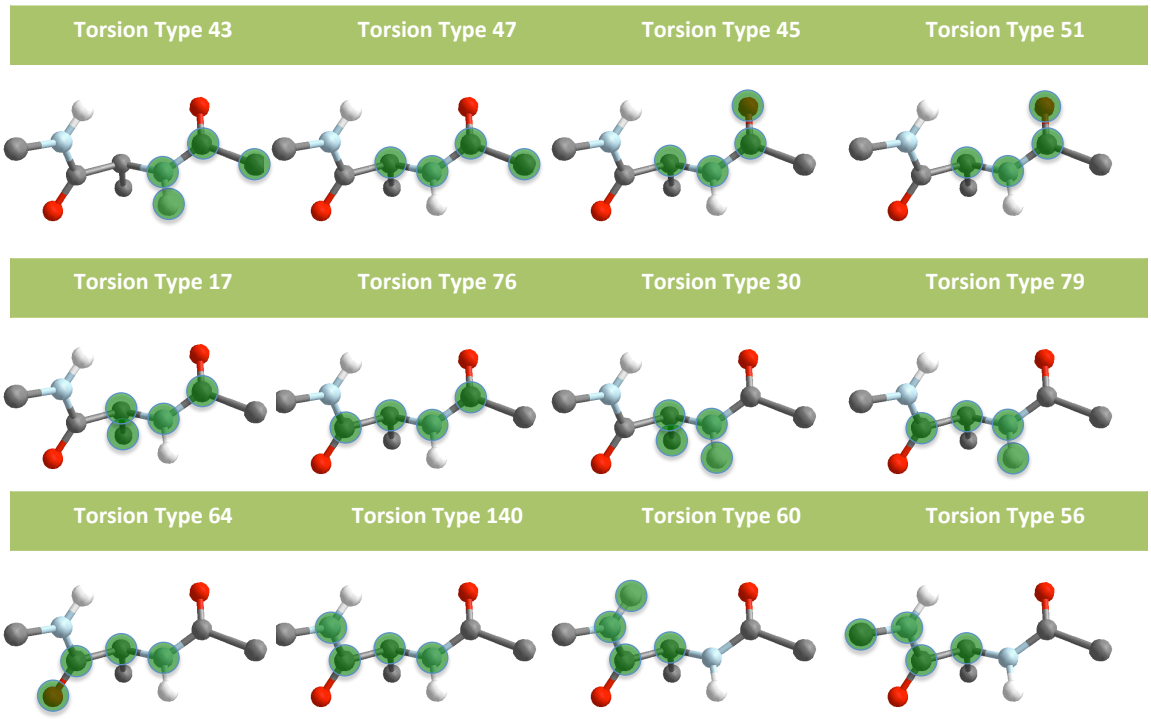

Figure 5: Sampled torsions. In green circles we show the four atoms that are active in a particular torsion. Sometimes torsion parameters are modeled only according to the central two atoms. Here we take the broader view and consider torsions with even one of the four atoms different as distinct.

The Pentapeptide WH5

We applied the POP method also to the pentapeptide Ac-WAAAH-NH_2 (WH5) with the aim of reproducing the experimental helical fraction as a function of the temperature. WH5 is forming an α-helical turn efficiently and rapidly [38]. WH5 consists of only 5 amino acids, i.e. a minimum number of amino acids to form a complete turn of an α helix. Its secondary structure has been determined by nuclear magnetic resonance (NMR) and circular dichroism (CD) and the kinetics of the helix ↔coil transition has been studied by T-jump experiments [39]. The cited reference reports the far UV CD spectra of WH5 and the derived helical fraction as a function of temperature. The small size of WH5 and its fast kinetics make this molecule the ideal candidate to undergo optimization by POP. The required sampling of conformational space should not be a problem for modern computer hardware and software.

Experimental setup: helical fraction

WH5 is a shortcut for the blocked peptide Ac-WA_3H^+-NH_2, (the histidine is in its protonated form) which was studied experimentally [39-41] and computationally [38,40] as a model for the formation of a single helical turn and minimal secondary structure. We seek parameterization of the potential for this peptide that reproduces a critical experimental curve for this system, the temperature dependent helical fraction [38]. The

simulation setup was the same as for alanine dipeptide unless explicitly stated otherwise. The program MOIL in its GPU version [15] was used in the simulation. The all atom version of the OPLS force field [42] (OPLSAA) started the optimization procedure. The molecule was solvated with 851 TIP3P water molecules in a periodic box size of 30.6 $Å^3$ and the simulations were conducted in the NVT ensemble using velocity scaling. The Particle Mesh Ewald grid was 32x32x32.

Simulations were run at temperatures 280, 300, 320 K for 360 ns each optimization cycle. Each picosecond of simulation a structure was recorded and saved. The program POP processed the collected structures. It computes the helical fraction and its derivative with respect to the parameters and modifies the parameters. The process was iterated 4 times following the algorithm of Table 1, always using the same three temperatures and the same time of simulation (360 ns).

Experimental setup: melting curve

The helical fraction is an integrated measure over a range of temperatures. It does not capture the shape of the melting curve or the melting temperature. To study the last we also consider as a target function the derivative of the helical content as a function of temperature. The simulation parameters were the same as before except that twelve temperatures equally distributed between 280 and 390K were considered and replica exchange simulations were used [29,30]. Temperature swaps were attempted each 10 steps.

The average running time between two temperature swaps was ~2.8 ps. This time the simulations were run for 400 ns for each step of parameter optimization

Results

The experimentally determined helical fraction for WH5 is reproduced from the experimental data of reference [38] and is shown in Figure 6 in the temperature range 280-360. In reference [38] the CD spectra was empirically matched against known fingerprints of a helix spectrum. The match provided the plot of helical content in Fig 6. The curve is similar in its overall shape to the melting curve measured for the peptide $(AAQAA)_3$ by NMR [43] . The experimental helical fraction decays from 56% to almost zero. We focus on three temperatures 280 K, 300 K, 320 K and conduct the required simulations as described in the setup section.

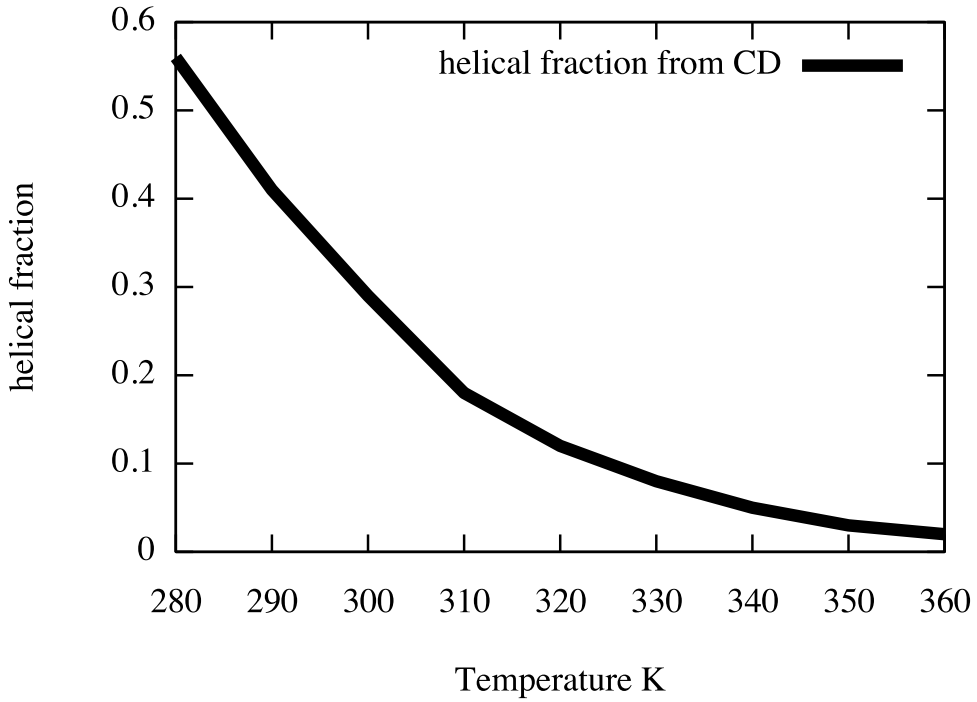

Figure 6: Experimentally measured fraction of helix conformation for WH5 . See text for more details.

In general, the average value of the (φ,ψ) angles for the α-helix is peaked near the point $(-62^{\circ},-41^{\circ})$; we considered an amino acid to be in a helical conformation if its backbone dihedral angles fall in a circle of radius 20° from the ideal value. Other definitions are possible. In the Lifson-Roig model emphasis is made on hydrogen bonding and therefore a helix is defined if three sequential amino acids are in the helical state. It is not clear if this is the appropriate definition for CD spectra. We therefore try them both. Below we present the result only for the single-amino acid definition. The use

of three (φ,ψ) pairs does not improve the results.

We define our microscopic observable $O(x,p)$ to be the helical fraction:

$$H(x)=\frac{N_{helix}}{N_{total}} \tag{3.9}$$

where N_{helix} is the number of amino acids in helical conformation and N_{total} is the total number of amino acids (5 for WH5).

As shown in Figure 7, in this temperature range the simulation with the starting potential gave helical fractions that are at significant variance with experiment. First, the helical fraction calculated from the simulation is less than the experimental value over the complete temperature range. Second, $\langle H\rangle_{(OPLSAA,T)}$ doesn't exhibit the sharp dependence on temperature seen in the experimentally determined curve. The computational curve is almost constant in the range considered.

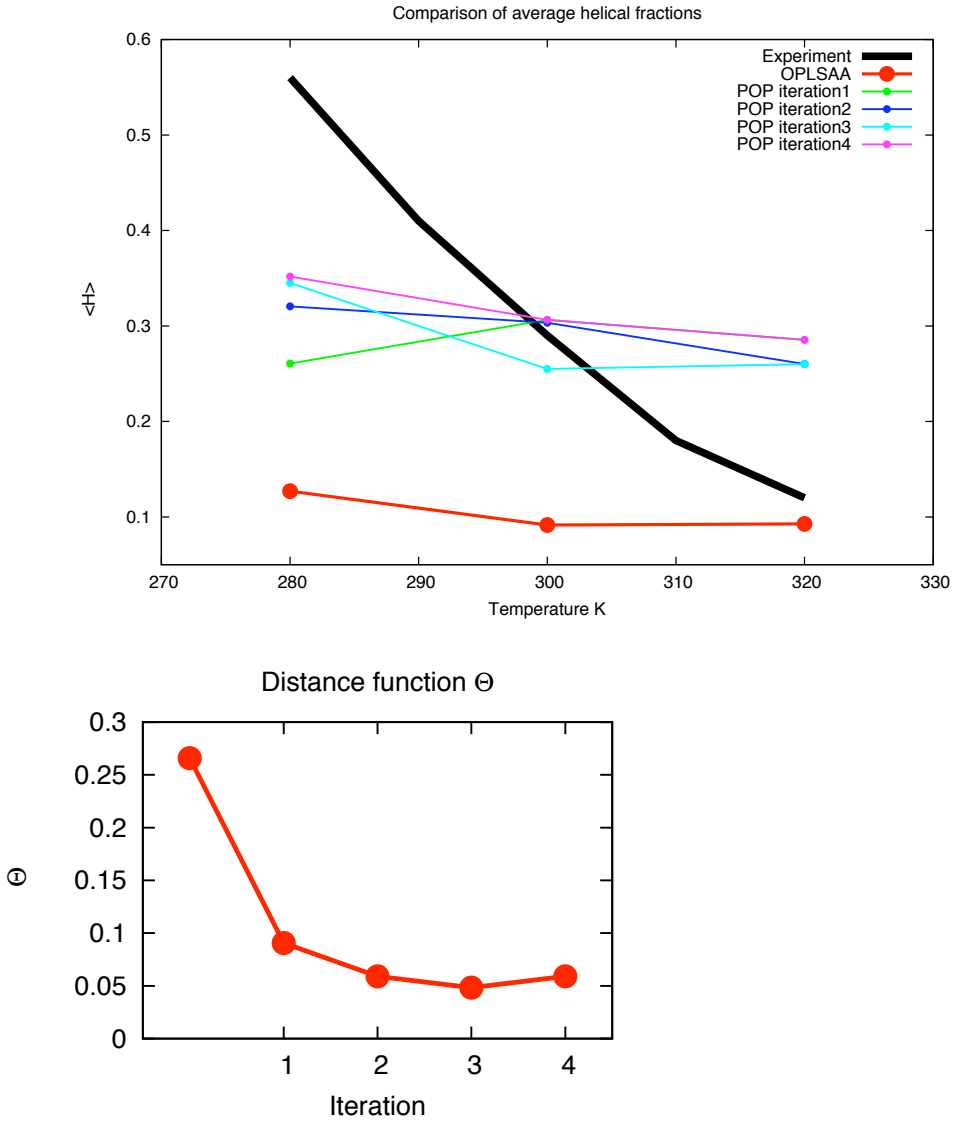

Figure 7: Top: A Comparison between the experimental folded fraction (black) and the results obtained from simulations with the OPLSAA force field (red) and optimized POP force fields. Down: Distance function $\Theta(\pi)$ as a function of the iteration

We defined the target function to be:

$$\Theta(\pi) = \sum_i \left(\langle H \rangle_{(\pi, T_i)} - H_{\text{experiment}}(T_i) \right)^2 \tag{3.10}$$

The index i is running over the three temperatures 280, 300 and 320 K.

POP optimization was performed on the Van der Waals and torsions parameters to minimize $\Theta(\pi)$; water parameters and charges were left untouched. After the first iteration the helical fraction was significantly improved reproducing the correct value at ~300 K (Figure 7). Three more POP iterations were performed with no substantial improvement; correct temperature dependence (or the overall shape of the melting curve) of the *in silico* helical fraction could not be achieved. The optimization process acted mostly on the parameters of the 207 torsions present in the molecule, thus confirming the intuitive idea that the helical fraction mostly depends on torsions; not one of the Lennard Jones parameters was modified more the 0.1%.

Remarkably, the changes in torsions parameters were small too. The molecule has 207 torsions subdivided in 97 torsion-types. Of 97 torsion-types just 7 had parameters modified in the range 5-10%, 9 torsions had parameters modified in the range 2-5% while the rest had changes less than 2%. These small, distributed changes in the parameter's set had a large effect on the helical fraction increasing it by more than a factor 2, Figure 8.

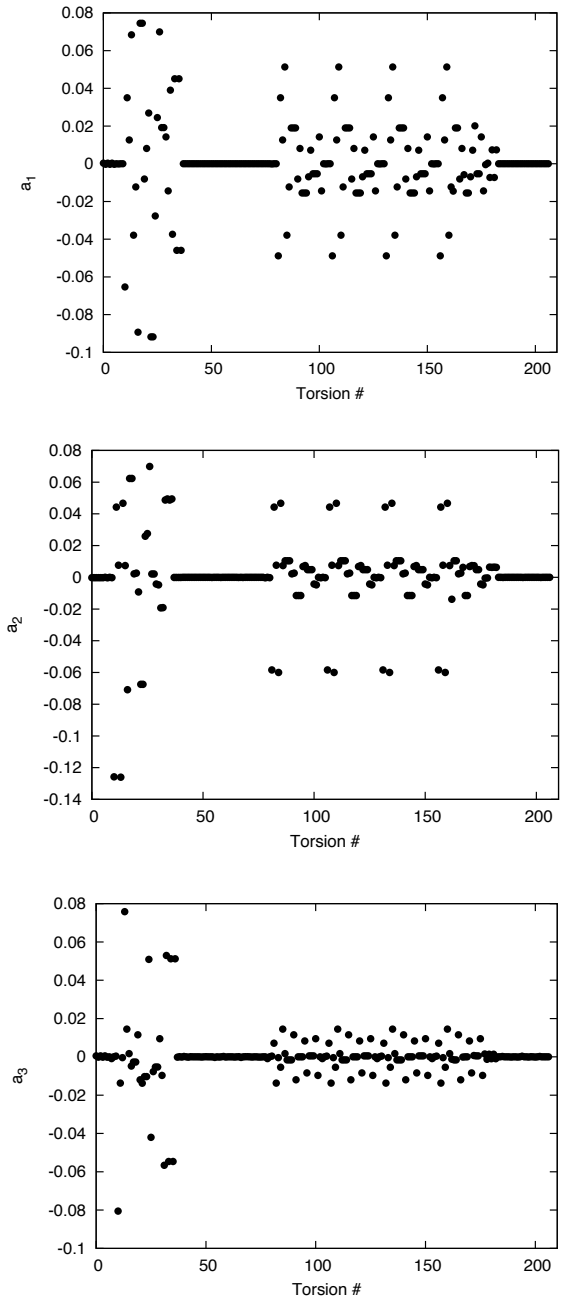

Figure 8: The difference in the coefficients of the torsion potential (a_1, a_2, a_3) of the OPLS-AA and POP potentials. The differences are small but they cause significant changes in helical content. Note that all torsions are displayed, which means that torsion types that repeat are shown more than once. The zero differences are mostly for side chain torsions.

Figure 9 shows the probability density of all the 5 amino acids of WH5 in different positions of the Ramachandran Map. The figure shows a comparison of probability densities for the starting and optimized force fields. The calculation presented is at temperature 300K. The result of the optimization is (as designed) an increased population of helical conformations. The differences between the two probability densities are also reported.

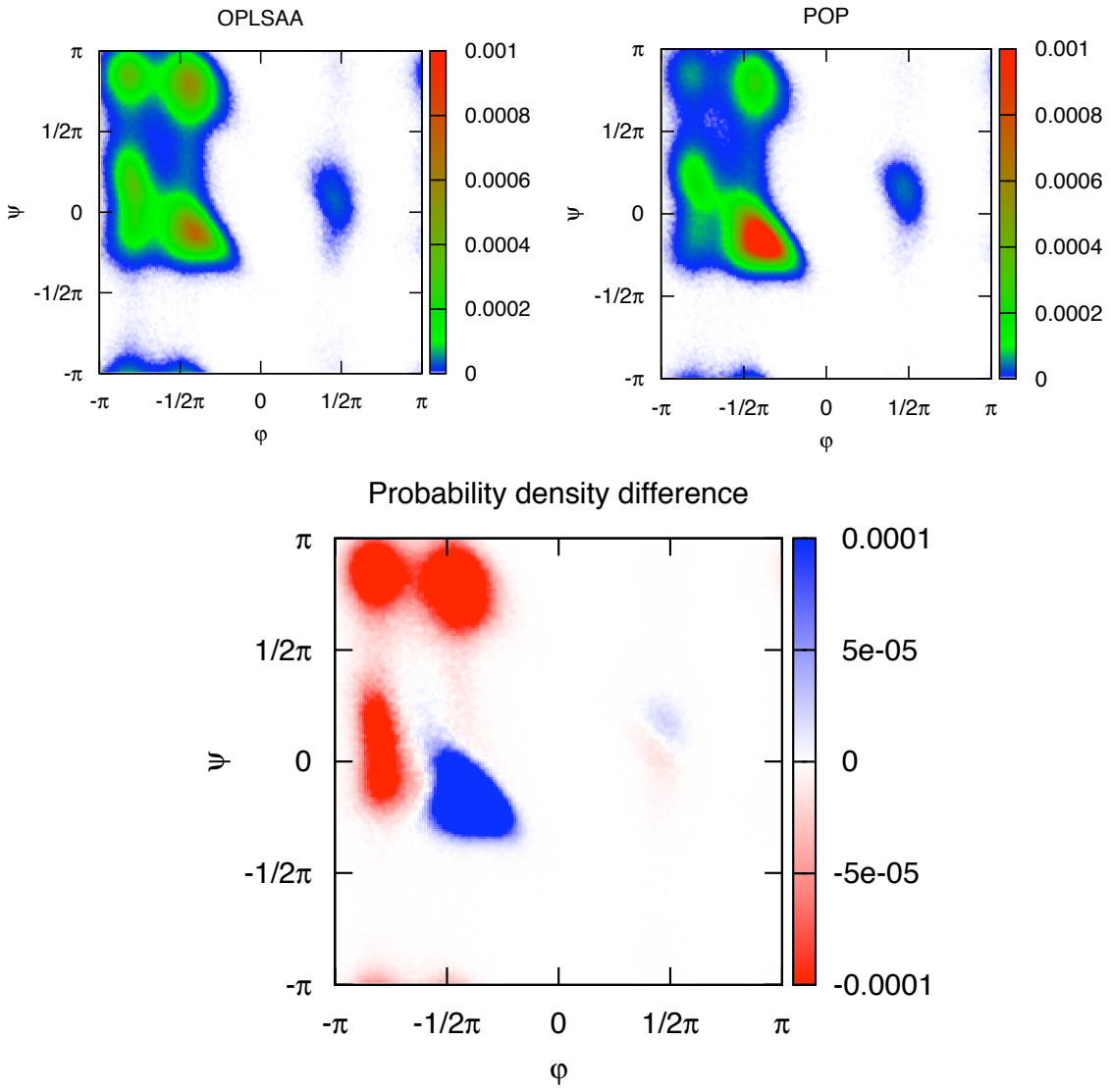

Figure 9: The three graphs show the probability density of finding any of the amino acids of WH5 in a given configuration defined by its dihedral backbone angles. The top figures show the probability density calculated at 300K from the potential OPLSAA and from the optimized potential POP (iteration 4). The lower figure shows the probability density difference between the two force fields. The probability density is normalized with respect to integration over the dihedrals φ and ψ .

A second attempt to optimize the shape of the melting curve was made by modifying the target function. We focused not on the helical fraction but on its derivative with respect to the temperature. We defined the target function to be:

$$\Theta(\pi) = \sum_{1}^{2} \left(D_{(i,\pi)} - D_{(i,\text{experiment})} \right)^2$$
$$D_{(i,\pi)} = \frac{\langle H \rangle_{(\pi,T_{i+1})} - \langle H \rangle_{(\pi,T_i)}}{T_{i+1} - T_i} \qquad (3.11)$$
$$D_{(i,\text{experiment})} = \frac{H_{\text{experiment}}(T_{i+1}) - H_{\text{experiment}}(T_i)}{T_{i+1} - T_i}$$

Where T_1, T_2, T_3 are, as before, the temperatures 280,300 and 320 K. We are therefore optimizing the numerical derivative of the helical fraction with respect to the temperature calculated at the two mid-temperatures 290, 310 K.

The convergence of the sensitivity was verified using independent simulations. Two molecular dynamics trajectories generate configurations to compute the average and the derivatives independently for each of the trajectories. Figure 10 illustrates the high correlations between the vectors of derivatives suggesting that the calculations of the derivatives indeed converge.

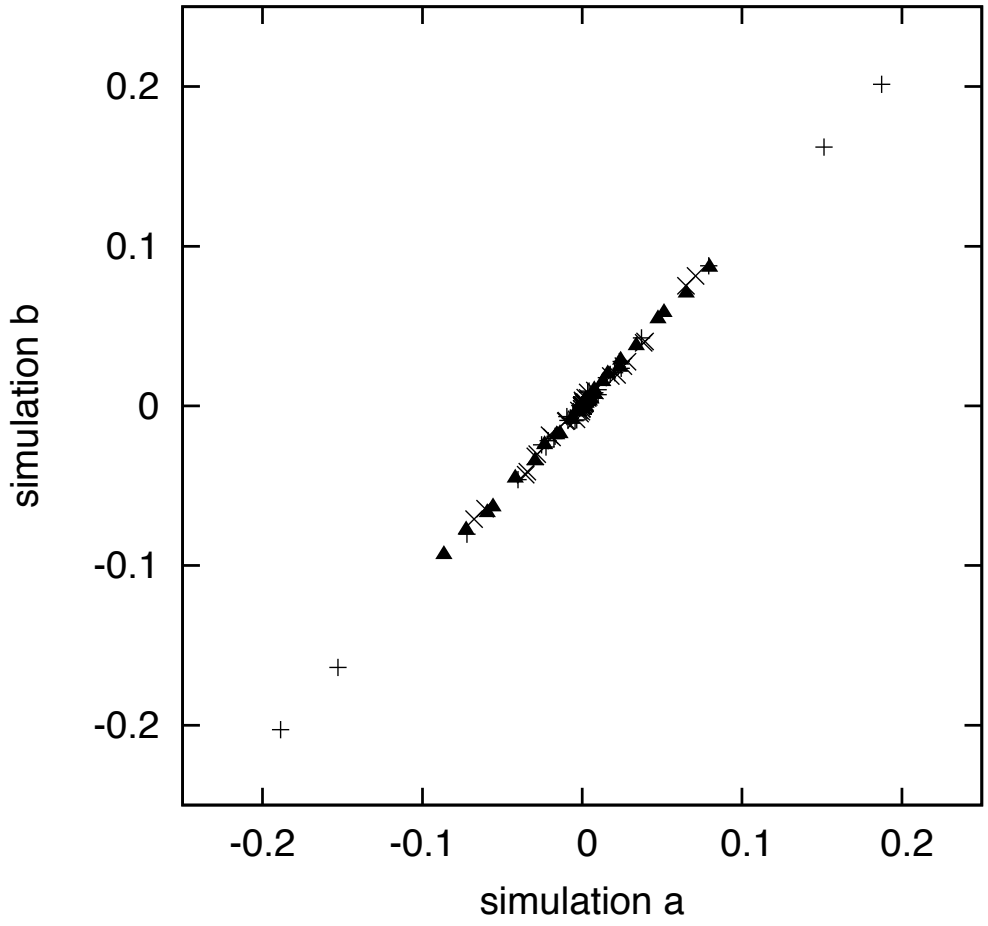

Figure 10: The gradient of the target function computed by ensemble averages of two simulations. We plot the correlation between the two gradients in which every element of the gradient vector is projected onto the axes to obtain the gradient value at each simulation. The high quality linear correlation suggests convergence.

The final value of the target function is $\Theta = 2.6 \times 10^{-4}$. No further improvement in the target function was obtained and the slope was not improving with additional cycles. We concluded that within the error bars of the potential parameters it is not

possible to adjust the shape of the melting curve.

Conclusions

We found that the helical content was a highly sensitive function of the backbone torsion parameters. In a way this is good news since the optimization of existing potentials to obtain the correct helical content is not difficult, provided that the direction of parameter changes is chosen correctly. Only minute adjustments in the potential parameters are required in order to bring the system to the correct conformations in equilibrium. Since the changes in the parameters are small it is likely that other observables will not be affected. A concern is however of transferability. If indeed such small adjustment in parameters cause such large shift in helical content, it is likely that transferability to other peptide systems (and proteins) would be hard to achieve since different peptides may require other small adjustments.

Another interesting observation in the simulation of WH5 is our inability to reproduce the melting curve of the peptide. These widely used experimental curves to determine stability energies and entropies of protein folding are insensitive functions of the parameters at hand. In fact, we gave up on the optimization since the procedure we use did not seem to make progress. We stress that our failure is relevant also to single temperature properties since quantities like entropy are related to the derivatives of the free energy and hence are incorrect.

The failure of our efforts to produce a potential that correctly predicts the melting curve discourages us from testing it on other systems. This negative result is supported by other attempts in the field to understand the unusual stability of short helices and to adjust force fields to reproduce this experimental observation. Arguments were made in the past that interactions with charged side chains add to the strong co-operativity of the helix [44,45]. The current optimization does not include all types of side chains and hence our exploration is limited. Nevertheless, some coupling of the backbone conformation is observed for the side chain torsion of tryptophan, supporting general interaction of side chains to backbone [46].

A number of extensions to the standard force field were proposed in the past. First, the water model (which we held fixed) may be inappropriate for a range of temperatures. Water models as TIP4P [47] and TIP5P [48], as well as a polarizable water model [49] are of significant promise since they better describe water properties and water anomalies. An interesting study was published by Best and Mittal [50] that illustrated the complexity of the task. The use of TIP4P/2005 [51] showed moderate improvement after the peptide potential was re-parameterized. Hence the peptide parameters are strongly coupled to the water model, which in most force fields are fitted against TIP3P or a similar model. Second, adjustments to the backbone torsion potentials were made. The CMAP approach has shown promise and the progress is encouraging [46,52,53] . In the CMAP approach a coupling between the (ϕ,ψ) dihedral angles is introduced, taking into account experimentally determined protein structures. This term is added to the usual Fourier expansion of the torsion energies that considers a torsion at a time. Another extension was proposed by Sakae and Okamoto [54] in which the torsion energy is made dependent on the amino acid type. The last approach, however, was not illustrated to improve peptide-melting curves. Third, polarizable force fields [55,56] may also play a

future role, and their evaluation is desired.

Finally we make a cautionary remark. While our results support the designs beyond the standard force field, they are a conjecture and not a proof. Our sampling of parameter space is incomplete. The optimization is based on a local minimization in which a nearby optimum of the target function is searched with a minimal change in the parameter values. The parameter space is rather smooth (especially compared to the coordinate space) since the energy dependence on the parameters that we optimize is either linear (torsion) or quadratic (Lennard Jones). For simple (quadratic) target functions the local minimization is exact. However, the Boltzmann factor makes the target function more complex and if exploration of multiple minima is required we will miss alternative stable states in parameter space.

POP applied to liquid mixtures[d]

Liquid mixtures are of great importance in chemical and petroleum engineering. Unfortunately, their properties are generally not well reproduced in simulation; this is a result of the parameterization procedure that is targeted to reproduce properties of pure liquids.

In this chapter we will develop a systematic scheme for the improvement of the computational modeling of liquid mixtures. In order to use POP to improve the parameterization of liquid mixtures we need observables that could give a computational characterization of the mixture and we need to relate such characterization to available experimental measurements. The Kirkwood-Buff theory of mixtures provides the needed connection between structural properties, easy to measure *in silico*, and thermodynamical properties easy to determine experimentally. We dedicate the first section to summarize this theory. Successively, we define the Kirkwood-Buff observables so that POP can use them as targets for optimization.

Finally we apply POP to obtain a force field for mixtures of water and the alcohol tert-butanol. The final force field is a successful force field for the molecule tert-butanol

---

[d] Part of the content of this chapter was previously published in collaboration with Ron Elber and M.L.Mugnai in

Di Pierro et al. (2014). "*Optimizing Potentials for a Liquid Mixture: A New Force Field for a tert-Butanol and Water Solution*." *J. Phys. Chem. B*, Article ASAP, **DOI:** 10.1021/jp505401m

Ron Elber supervised the work; M.L. Mugnai contributed to the adaptation of the KB theory and provided part of the simulation data.

that reproduces extremely well the KB integrals. POP has obtained it in an automated way in only 4 iterations.

Kirkwood-Buff Theory

The Kirkwood-Buff (KB) theory of fluid mixtures[18] relates some integrals of the pair correlation functions (microscopic observables) computed in the grand-canonical ensemble, to derivatives of the chemical potential, isothermal compressibility and partial molar volumes (macroscopic quantities). A detailed derivation of the theory can be found elsewhere.[18,57] Here, we present the key concepts for our application. The use of KB to optimize potential parameters was put forward by Smith.[58] The automated optimization using Newton Raphson in a trusted region is our contribution.

Let's consider a binary mixture of two chemical species, chemical species "S1" and chemical species "S2". The symbols "A" and "B" can either be "S1" or "S2". Let's define the following pair correlation function:

$$g_{AB}^{\mu_1\mu_2 VT}\left(\vec{r}_1,\vec{r}_2\right)=\frac{\rho_{AB}^{\mu_1\mu_2 VT}\left(\vec{r}_1,\vec{r}_2\right)}{\rho_A^{\mu_1\mu_2 VT}\left(\vec{r}_1\right)\ \rho_B^{\mu_1\mu_2 VT}\left(\vec{r}_2\right)}=\frac{\left\langle\sum_{i\in A}\sum_{j\in B}\delta\left(\vec{r}_1-\vec{r}_i\right)\delta\left(\vec{r}_2-\vec{r}_j\right)\right\rangle_{\mu_1\mu_2 VT}}{\left\langle\sum_{i\in A}\delta\left(\vec{r}_1-\vec{r}_i\right)\right\rangle_{\mu_1\mu_2 VT}\left\langle\sum_{j\in B}\delta\left(\vec{r}_2-\vec{r}_j\right)\right\rangle_{\mu_1\mu_2 VT}} \quad (4.1)$$

The averages are performed in the grand-canonical ensemble (holding fixed the reservoir's temperature T, the volume V, and the chemical potentials of the two chemical species "S1" and "S2" are μ_1 and μ_2, respectively). This function expresses the joint probability of finding the center of mass of a molecule of species A (we indicate its position by $\vec{r}_i$) at $\vec{r}_1$ and the center of mass of a molecule of species B (we indicate its position by $\vec{r}_j$) at $\vec{r}_2$, relative to the probability of the two independent events. Note that, even though only the centers of mass appear in equation (4.1), the theory is general: it does not require spherically symmetric molecules. Indeed, the internal degrees of freedom of A and B molecules, as well as their overall orientation, are accounted for in the ensemble average.[18,57]

Let's assume that the system is homogeneous, and so that the probability of finding a molecule in a specific place is constant anywhere in the system. In this case, we can rewrite (4.1) as:

$$g_{AB}^{\mu_1\mu_2VT}\left(\vec{r}_1-\vec{r}_2\right)=\frac{\left\langle\sum_{i\in A}\sum_{j\in B}\frac{1}{V}\delta\left(\vec{r}_1-\vec{r}_2-\vec{r}_i+\vec{r}_j\right)\right\rangle_{\mu_1\mu_2VT}}{\left\langle\sum_{i\in A}\frac{1}{V}\right\rangle_{\mu_1\mu_2VT}\left\langle\sum_{j\in B}\frac{1}{V}\right\rangle_{\mu_1\mu_2VT}}= \\ =\frac{\frac{1}{V}\left\langle\sum_{i\in A}\sum_{j\in B}\delta\left(\vec{r}_1-\vec{r}_2-\vec{r}_i+\vec{r}_j\right)\right\rangle_{\mu_1\mu_2VT}}{\frac{\left\langle N_A\right\rangle_{\mu_1\mu_2VT}}{V}\frac{\left\langle N_B\right\rangle_{\mu_1\mu_2VT}}{V}}=\frac{\rho_{AB}^{\mu_1\mu_2VT}\left(\vec{r}_1-\vec{r}_2\right)}{\rho_A^{\mu_1\mu_2VT}\rho_B^{\mu_1\mu_2VT}} \tag{4.2}$$

Let's now define $\vec{r} = \vec{r}_1 - \vec{r}_2$ and $\vec{r}_{ij} = \vec{r}_i - \vec{r}_j$. If the probability of finding the center of mass of B-type molecules around a molecule of species A depends only on their distance, and not the orientation of the vector that connects them (i.e. the system, averaged over its internal degrees of freedom and the orientations of the molecules, is isotropic) then we can rewrite (4.2) as:

$$g_{AB}^{\mu_1\mu_2 VT}(r) = \frac{\rho_{AB}^{\mu_1\mu_2 VT}(r)}{\rho_A^{\mu_1\mu_2 VT}\rho_B^{\mu_1\mu_2 VT}} = \frac{1}{V}\frac{\left\langle \sum_{i\in A}\sum_{j\in B}\frac{1}{4\pi r^2}\delta\left(r - r_{ij}\right)\right\rangle_{\mu_1\mu_2 VT}}{\rho_A^{\mu_1\mu_2 VT}\rho_B^{\mu_1\mu_2 VT}} \tag{4.3}$$

where we transformed the Dirac's delta from Cartesian coordinates to polar coordinates.

The key object in the KB theory is the so-called KB integral:

$$G_{AB}^{\mu_1\mu_2 VT} = \int_V d\vec{r}\left[g_{AB}^{\mu_1\mu_2 VT}(r) - 1\right] \tag{4.4}$$

The meaning of this quantity becomes clearer if we rewrite equation (4.4) as:

$$\rho_B^{\mu_1\mu_2 VT} G_{AB}^{\mu_1\mu_2 VT} = \int_V d\vec{r}\left[\frac{\rho_{AB}^{\mu_1\mu_2 VT}(r)}{\rho_A^{\mu_1\mu_2 VT}} - \rho_B^{\mu_1\mu_2 VT}\right] \tag{4.5}$$

The left hand side of equation (4.5) is the so-called excess coordination number. The integrand in the right hand side of equation (4.5) has two terms: first the conditional probability of finding a molecule of species B around a molecule of species A, second the probability of finding the molecule of species B. The integral gives the excess (or shortage) of molecules of species B in volume V around a molecule of species A with respect to the average number of B-type molecules in the same volume V. Obviously, at large distances (for small solutes typically a few nanometers), the correlation between A-type and B-type molecules is lost (i.e. $\rho_{AB}^{\mu_1\mu_2VT}(r) \underset{r\to\infty}{\to} \rho_A^{\mu_1\mu_2VT}\rho_B^{\mu_1\mu_2VT}$) and the integrand of (4.5) is zero. This means that the KB integral carries local, microscopic information that can be evaluated with a MD simulation.

At the same time, it is possible to show[18,57] that the KB integral (4.4) is equal to:

$$G_{AB}^{\mu_1\mu_2VT} = V\left[\frac{\langle N_A N_B\rangle_{\mu_1\mu_2VT} - \langle N_A\rangle_{\mu_1\mu_2VT}\langle N_A\rangle_{\mu_1\mu_2VT}}{\langle N_A\rangle_{\mu_1\mu_2VT}\langle N_B\rangle_{\mu_1\mu_2VT}} - \frac{\delta_{AB}}{\langle N_A\rangle_{\mu_1\mu_2VT}}\right] \tag{4.6}$$

where N_A and N_B are the number of molecules of type A and B, respectively, and δ_{AB} is the usual Kronecker's delta.

This equation expresses the connection with thermodynamics. The fluctuation of numbers of particles in the system is a macroscopic object, and it can be expressed in terms of derivatives of the chemical potential of A-type molecules with respect to number of particles of species B, isothermal compressibility and partial molar volumes of the two

species.[18,57] These quantities can be measured experimentally. It is also possible to extract the KB integrals from these thermodynamical quantities.[59]

Therefore, KB theory provides a useful protocol to analyze MD simulation and connect the results with measurable quantities: it requires extracting from the trajectory the pair correlation function and its integral, which are routinely computed. Indeed, it has been found in numerous applications in recent years, particularly in the context of force field parameterization.[19-21,60-62]

Nevertheless, there are some caveats. First of all, MD simulations are performed at constant number of particles, so in the canonical, not in the grand-canonical ensemble. The connection between the KB integral and the measurable quantities relies upon equation (4.6), which in the canonical ensemble would be:[57]

$$G_{AB}^{N_1 N_2 VT} = -V\frac{\delta_{AB}}{N_A} \tag{4.7}$$

where N_1 and N_2 are the fixed number of particles of species "S1" and "S2", respectively.

Obviously, in this case, the connection with the chemical potential would be lost. How can we compute a grand-canonical average from a canonical simulation? A possible way is to compute the KB integral in a volume V' that is much smaller than the volume of the system. In such volume, the number of molecules fluctuates. The rest of the system acts as a molecular reservoir. This procedure is correct as long as the pair correlation function in (4.4) decays to 1 within V'. This leads to the second caveat: sometimes the pair correlation function decays to 1 very slowly and we need to account properly for its

long tail. A careless truncation may have a bad impact on the evaluation of the KB integral. To understand why, let's consider the case in which the KB integral in (4.4) is computed in a spherical domain of radius R_C:

$$G_{AB}^{\mu_1\mu_2 VT}(R_C) = \int_0^{R_C} \left[g_{AB}^{\mu_1\mu_2 VT}(r) - 1 \right] 4\pi r^2 dr \tag{4.8}$$

If at R_C the pair correlation function is not 1, we are neglecting a contribution to the integral that might potentially be very large as it is multiplied by the square of the radius.

Ganguly and van der Vegt[63] have investigated these caveats and proposed empirical corrections to the KB integrals to alleviate these problems. Others[64] have carried out the calculation of KB integrals using the Adaptive Resolution Scheme for MD.[65] In our case we decided to compute the integral of the pair correlation in the NVT ensemble without corrections, but we computed the integral of the pair correlation function up to 20Å, which is large compared with what is commonly found in literature.[19-21,63] In this way we can check whether the KB integral has indeed reached a plateau. To ensure that the system can be considered grand-canonical, we run the simulations in cubic systems of roughly 65Å box length. This ensures that the reservoir is around 7 times larger than the volume V' in which the pair correlation function is computed.

The Kirkwood-Buff observable functions

In this chapter we use the method described above to optimize the MD force field using the three KB integrals of a binary liquid mixture as a target for optimization. We write an observable function associated with the KB integrals. We derive the observable function from the definition of the KB integral; using equation (4.3) for the pair correlation function but computed in the canonical ensemble, we obtain:

$$G^{(N,V,T,\pi)}{}_{AB}\left(R_C\right) = \int_0^{R_C} \left[g_{AB}(r) - 1\right] 4\pi r^2 \, dr = \left\langle \int_0^{R_C} \sum_{\substack{i \in A \\ j \in B}} \frac{1}{\rho_A \rho_B V} \delta\left(\left|\vec{r}_i - \vec{r}_j\right| - r\right) dr \right\rangle_{(N,V,T,\pi)} - \frac{4}{3}\pi R^3{}_C \tag{4.9}$$

The function inside the canonical ensemble average is our observable; in this case it only depends on the set of all coordinates $\mathbf{R}$. We define our observable functions to be:

$$O_1(\mathbf{R}) = \int_0^{R_C} \sum_{\substack{i\in S1 \\ j\in S2}} \frac{1}{\rho_1\rho_2 V}\delta\left(\left|\vec{r}_i - \vec{r}_j\right| - r\right)dr - \frac{4}{3}\pi R^3{}_C$$

$$O_2(\mathbf{R}) = \int_0^{R_C} \sum_{\substack{i\in S1 \\ j\in S1}} \frac{1}{\rho_1\rho_1 V}\delta\left(\left|\vec{r}_i - \vec{r}_j\right| - r\right)dr - \frac{4}{3}\pi R^3{}_C \qquad (4.10)$$

$$O_3(\mathbf{R}) = \int_0^{R_C} \sum_{\substack{i\in S2 \\ j\in S2}} \frac{1}{\rho_2\rho_2 V}\delta\left(\left|\vec{r}_i - \vec{r}_j\right| - r\right)dr - \frac{4}{3}\pi R^3{}_C$$

where $\rho_1 = \frac{N_1}{V}$ and $\rho_2 = \frac{N_2}{V}$.

Let's define

$$\overline{\left(N_B(R_C) \mid A\right)}(\mathbf{R}) = \frac{1}{N_A}\sum_{\substack{i\in A \\ j\in B}} \int_0^{R_C} \delta\left(\left|\vec{r}_i - \vec{r}_j\right| - r\right)dr \qquad (4.11)$$

i.e. the number of molecules of species B which are at distance less than R_C from a molecule of species A averaged on all the molecules of species A. Similarly, we can define

$$\overline{\left(N_A(R_C)\right)} = \rho_A \frac{4}{3}\pi R^3{}_C \qquad (4.12)$$

the average number of molecules in a spherical volume of radius R_C . We can rewrite equation (4.10) as:

$$
\begin{aligned}
O_1(\mathbf{R}) &= \frac{1}{\rho_2}\left[\overline{\left(N_2(R_C) \mid S1\right)}(\mathbf{R}) - \overline{\left(N_2(R_C)\right)}\right] = \frac{1}{\rho_1}\left[\overline{\left(N_1(R_C) \mid S2\right)}(\mathbf{R}) - \overline{\left(N_1(R_C)\right)}\right] \\
O_2(\mathbf{R}) &= \frac{1}{\rho_1}\left[\overline{\left(N_1(R_C) \mid S1\right)}(\mathbf{R}) - \overline{\left(N_1(R_C)\right)}\right] \\
O_3(\mathbf{R}) &= \frac{1}{\rho_2}\left[\overline{\left(N_2(R_C) \mid S2\right)}(\mathbf{R}) - \overline{\left(N_2(R_C)\right)}\right]
\end{aligned}
\tag{4.13}
$$

So, the observables in equation above (4.13) measure the excess (or shortage) of a molecule of type A around a molecule of type B compared to the average in the system. The observables do not carry explicit parameter dependence, which simplifies the expressions for the gradient and the Hessian. While the observable function depends explicitely only on the coordinates it is clear that its ensemble average depends on the composition of the liquid mixture. The ensemble average is a function of the variables $\left(N_1, N_2, V, T, \pi\right)$. If we introduce the molar fraction

$$
x = \frac{N_1}{N_1 + N_2} \ , \qquad N = N_1 + N_2
$$

the same set of variables can be written as $\left(N, x, V, T, \pi\right)$. In the following we are only interested in changes in parameters and molar fractions, we will therefore drop the other

variables; clearly, it is to be intended that experiment and computation are performed under the same conditions.

For multiple mole fractions N_x the target function is:

$$\Theta(\pi) = \sum_{j=1}^{N_x} \sum_{i=1}^{3} \left[\langle O_i \rangle_{(x_j,\pi)} - O_{\exp,i}\left(x_j\right) \right]^2 \tag{4.14}$$

Setup: optimization

For the MD simulations a mixtures of tert-butanol (TBA) and water were prepared at the mole fractions of TBA in Table 2. The model used for water was TIP3P[23] and it remained fixed throughout the process of potential refinement. The starting model chosen for TBA was the OPLS united atom model (OPLSUA)[22]. The system was prepared to have density consistent with experiment (error of about one percent,[66] see Table 2). Particle Meshed Ewald (PME)[37] was used to account for long-range electrostatic interactions with a grid of 64x64x64. Short-range electrostatic interactions were calculated by real space summation up to a cutoff of 9.5 Å; the same cutoff was used for Van Der Waals interactions. Periodic boundary conditions were applied. The equation of motion were integrated using the multiple time-step integrator RESPA[34] with a time step of 1 fs. Short-range forces were updated every femtosecond while long range

interactions were calculated every 4 femtoseconds according to the protocol in MOIL described in [15]. The sampling in the NVT ensemble was enforced by rescaling the velocities (isokinetic ensemble [3]). The temperature was set to be 300K in all the simulations. The experimental results used in the target function are those in [24].

An iteration of the optimization of the potential parameters includes a series of MD simulations to collect a sample of structures. An ensemble of structures computed with a particular force field is analyzed to calculate the new parameter set. The new parameter set and potential are used in a successive MD simulation, from which we collect new structures that are analyzed again.

For the first three iterations the target function used was:

$$\Theta_{I-III}(\pi) = \sum_{i=1}^{3} \left[\langle O_i \rangle_{(x,\pi)} - O_{\exp,i}(x) \right]^2 \tag{4.15}$$

at the single mole fraction of TBA x=0.2.

For the last iteration we used the target function:

$$\Theta_{IV}(\pi) = \sum_{j=1}^{2} \sum_{i=1}^{3} \left[\langle O_i \rangle_{(x_j,\pi)} - O_{\exp,i}(x_j) \right]^2 \tag{4.16}$$

with mole fraction of TBA x_1 =0.04 and x_2=0.10.

The optimization process was stopped at the IV iteration, where the experimental observables matched the simulated quantities within acceptable error bars.

All the MD simulations were performed using the software package MOIL in its GPU variant [15]. The analysis of the structures, including the calculation of gradient and Hessian and the updating of the parameter set, was performed using the software POP [13] included in MOIL.

The Kirkwood-Buff integrals were calculated up to a cut-off distance of 20 Å. For each iteration, a simulation of 60 ns was performed. We discarded the initial equilibration phase (10 ns), and from the last 50 ns, we collected 4990 equally spaced (in time) structures. The structures were used in the calculations for parameter optimization by POP.

Setup: validation

To validate our potential we examine the performance of the newly developed model over a range of mixtures at different concentrations. We prepared 6 systems at mole fractions for which experimental results for the Kirkwood Integrals are known [24] (see Table 2). Each of the systems was simulated for 60 ns with the same setup described in the optimization paragraph and the experimental observables were compared to the simulations.

Table of concentrations

TBA Molar concentration	0.04	0.10	0.14	0.17	0.20	0.30
Density g/cm^3	0.9707	0.9357	0.9146	0.9010	0.8836	0.8577
Volume Å^3	64.079^3	64.393^3	64.723^3	64.987^3	65.255^3	66.170^3
Number of TBA molecules	304	637	808	919	1000	1289
Number of water molecules	7290	5733	4968	4488	4096	3006

Table 2: We report molar concentration of TBA, density, volumes and number of molecules of each one of the systems simulated. The parameters were chosen such that the densities were within a percent from the experimental values reported in reference [66] at 308.15K.

Force Fields

The starting force field for TBA is OPLSUA[22]. In this force field, TBA is composed of 6 particles, since each of the methyl group is treated as a single particle without internal degrees of freedom. Here, we report the OPLSUA force field and the optimized force field, which we will refer to as POP4ff.

The complete potential is a sum of bonding and non-bonding terms:

$$U_{total} = \sum_{b} U_b + \sum_{\theta} U_\theta + \sum_{\phi} U_\phi + \sum_{LJ} U_{LJ} + \sum_{elec} U_{elec}$$

The functional form for bonded terms (bonds, angles and torsions) is:

$$U_b = \frac{k_b}{2}\left(r - r_0\right)^2 \quad U_\theta = \frac{k_\theta}{2}\left(\theta - \theta_0\right)^2 \quad U_\phi = \sum_n K_n \cos\left(n\phi + \delta_n\right)$$

The non bonded terms (Lennard-Jones and electrostatic) are

$$U_{LJ} = 4\varepsilon_{ij}\left[\left(\frac{\sigma_{ij}}{r_{ij}}\right)^{12} - \left(\frac{\sigma_{ij}}{r_{ij}}\right)^{6}\right] \quad U_{elec} = k_{el}\frac{q_i q_j}{r_{ij}}$$

with combination rules:

$$\sigma_{ij} = \sqrt{\sigma_i \sigma_j} \qquad \varepsilon_{ij} = \sqrt{\varepsilon_i \varepsilon_j} \ .$$

Our software utilizes the equivalent formulation:

$$U_{LJ} = \left(\frac{A_i A_j}{r_{ij}^{12}}\right) - \left(\frac{B_i B_j}{r_{ij}^{6}}\right)$$

Some of the results will be presented with respect to parameters A and B. Angles and bonds parameters were not optimized and are therefore shared between OPLSUA and POP3ff.

The torsions parameters were optimized in POP4ff but are very similar to the one of OPLSUA; POP4ff final parameters were (K_1, K_2 ,K_3)=(0.0001,-0.0003,0.3258) while OPLS parameters are (K_1, K_2 ,K_3)=(0,0,0.325). Hence, in practice, only the amplitude of the three fold rotation is different from zero.

Bonded parameters

Bonds	k_b (kcal/mol Å²)	r_0 (Å)	
O-H	553.0	0.945	
C-O	320.0	1.430	
C-CH_3	268	1.530	
Angles	k_θ (kcal/mol)	θ_0	
CH_3–C-CH_3	63.0	112.00	
H-O-C	55.0	108.50	
O-C- CH_3	80.0	108.00	
Torsions	K_1 (kcal/mol)	K_2 (kcal/mol)	K_3 (kcal/mol)
H-O-C- CH_3	0	0	0.325

Table 3: Bonded parameters for united atom tert-butanol for the force field OPLS and POP4ff. Bonded terms are the standard OPLS force field. Angles and bonds were not optimized; the change in torsions parameters was found to be small during the calculations, and their adjustment is ignored.

Non-bonded parameters

OPLS parameters

Atom Type	q (*e*)	ε (kcal/mol)	σ (Å)
C	0.265	0.050	3.800
CH_3	0	0.160	3.910
O	-0.700	0.170	3.070
H	0.435	0	0

POP parameters

Atom Type	q (*e*)	ε (kcal/mol)	σ (Å)
C	0.04670	0.0372	3.9899
CH_3	0.10900	0.1271	4.0618
O	-0.58197	0.1566	3.1104
H	0.20827	0	0

Table 4: Non-bonded parameters for united atom tert-butanol for the force field OPLSUA and POP4ff.

Results and discussion

Tert-butanol (TBA) is a tertiary alcohol. Unlike the other butyl alcohols, TBA is miscible in water at any proportion and any temperature[67]; it is also the largest monohydric alcohol to be fully soluble [68]. TBA-water mixtures exhibit many anomalous physical properties. Solutions of TBA in water show an anomalously large volume contraction indicating that the tri-methyl groups must be somehow easily accommodated into the water structure [69]. There is evidence that TBA when added to water in solvating peptides behaves as helix promotor [70].

The peculiar characteristics of TBA motivate us to apply our newly developed procedure to investigate it and improve current potentials.

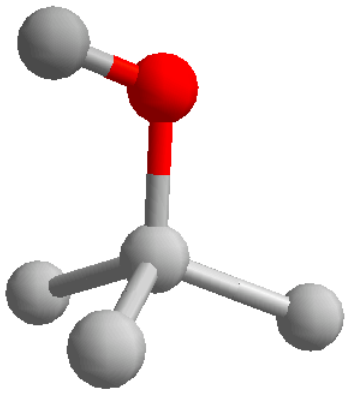

Figure 11: A united atom model of TBA; note that each methyl group is represented by a single united atom.

We first simulated the mixture of TBA and water using the parameters of the OPLSUA force field. After equilibration, phase separation is evident by visual inspection, as illustrated in Figure 12. This is a known effect, as force fields optimized to reproduce pure liquids properties often exhibit too much self-aggregation when observed in solution [71]. This system was the starting point of our optimization. In the same figure we show the same system once equilibrated with the optimized force field of the fourth iteration; we will refer to this force field as POP4ff.

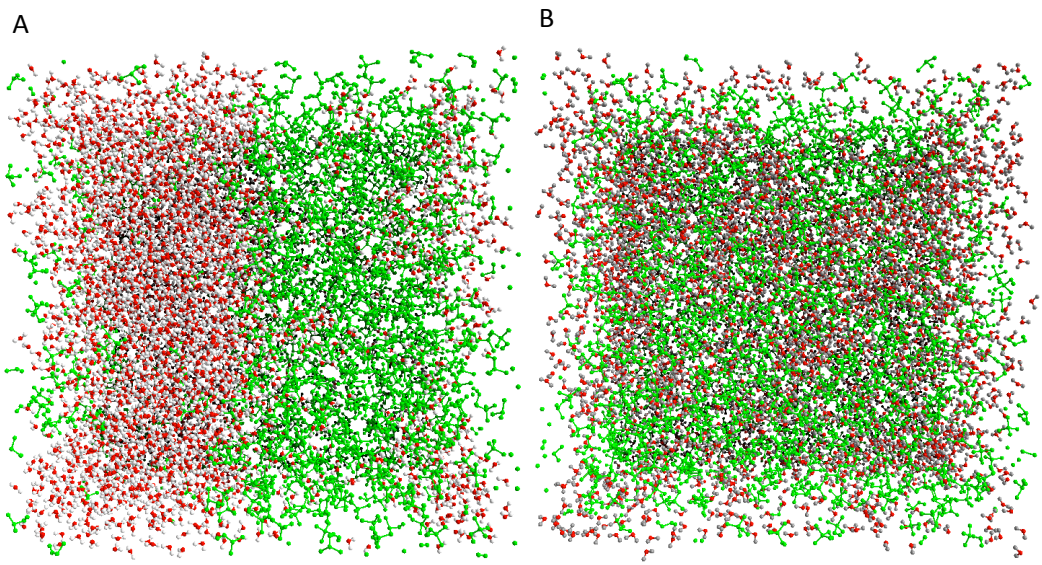

Figure 12: Snapshots of the simulation box; TBA is in green. On the left, we show an equilibrium snapshot of the mixture of TBA and water at 0.20 TBA mole fraction using the OPLSUA force field. Phase separation is evident by visual inspection. On the right, the same system after equilibration using POP4ff; by visual inspection the solution is mixed.

In the optimization we used KB integral extracted from Small-Angle X-ray Scattering[24]. In calculating the KB integrals from MD data we assumed the position of the oxygen atom to be the position of water molecule; similarly, the position of the tert-butanol molecule is assumed to be the one of the central carbon.

In Figure 13 we show the KB integrals for POP4ff as a function of the cutoff R_C

for all the concentrations tested in our simulations. At a distance of 20Å the integrals are approaching a plateau, suggesting that we are close to the region where the integral is converged.

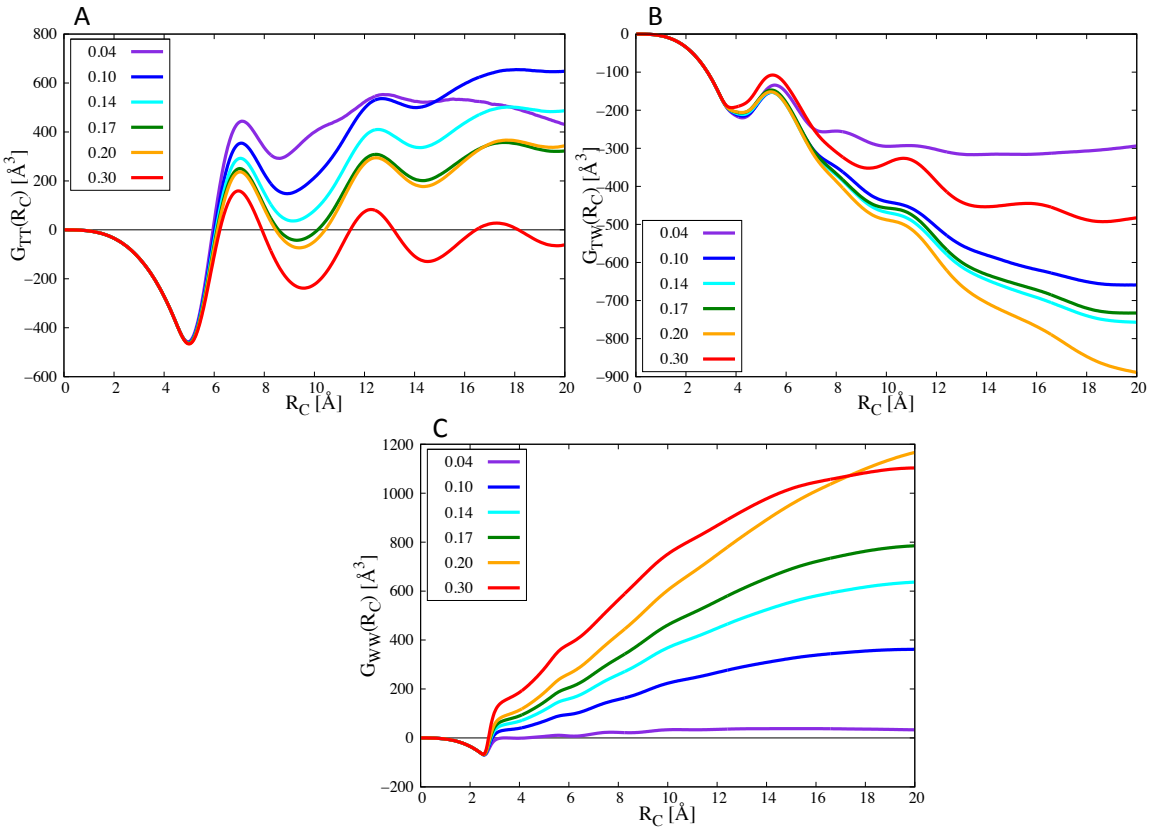

Figure 13: (A) The value of the KB integral of TBA-TBA as a function of RC (see equation (4.9)); (B) TBA-Water; (C) Water-Water. The mole fractions in Table 1 are displayed in different colors. At 20Å most of the curves are close to a plateau indicating convergence.

Lee and Van der Vegt[21] already used the KB theory to develop a force field for tert-butanol obtaining good results. They used the LJ parameters from GROMOS[72] and SPC[73] as a water model. They tuned the dipole moment of the tert-butanol molecule so that they could better reproduce the KB integrals over a range of concentration. Their protocol, while successful, shows the typical limitation of current force field development; they could adjust only a few parameters at the time. The choice of those parameters is left to chemical intuition. Some of the results were unphysical such as an extremely large Van der Waals radius for the central carbon.

We repeated the optimization of the force field in an automated procedure using KB integrals as optimization target for the POP algorithm. All the parameters (excluded bonds and angles) of the model were subject to automated optimization following the gradient. The tert-butanol molecule, in the united atoms model, is composed of 3 torsions (of 1 torsion type) and 6 atoms (of 4 different atom types). In OPLS polar hydrogen atoms have zero Van der Waals radius. We kept this convention and we did not optimize those parameters. The total number of parameters under optimization was 13.

Four iterations of the optimization procedure were conducted. The progression in approaching the experimental values through the optimization iterations is shown in figure 14.

The first three iterations were conducted using as a target the KB integrals of mole fraction of TBA 0.2. The first optimization step massively improved the original OPLSUA force field as it is shown in figure 14. Iteration II and III yielded smaller but significant improvements.

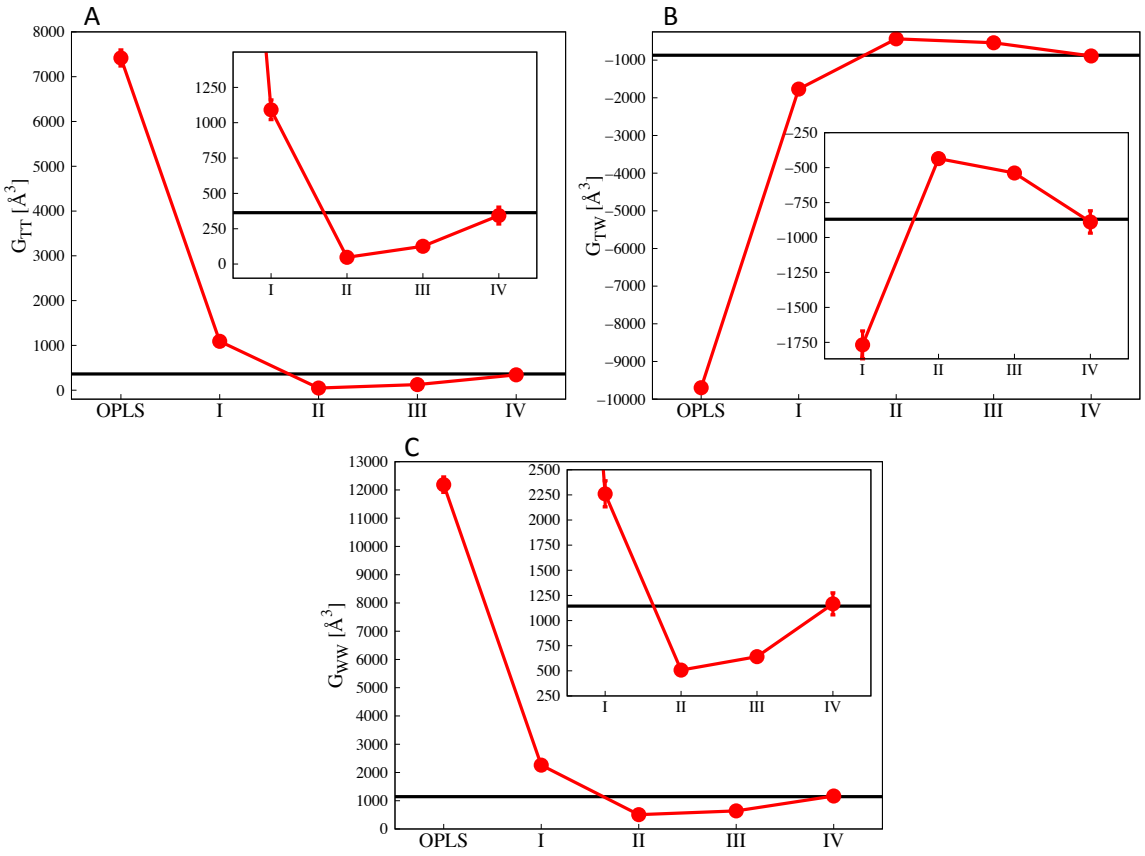

Figure 14: (A) KB integral for TBA-TBA at mole fraction of TBA 0.2 as a function of the optimization iteration. The first data point corresponds to the KB integral calculated with the force field OPLSUA.[22] The data point IV corresponds to the final force field POP4ff and the experimental value[24] is represented by the black horizontal line. In the inset the same data are shown with magnified scale for the last four data points. The error bars, computed with block analysis,[3] are sometimes below the size of the point. (B) and (C): same data for TBA-water and water-water; even in this cases the final force field reproduces the experimental value.

After the third iteration the optimization procedure produced only minor improvements. We therefore decided to use a more informative target function. Inspection of the results over a broader range of concentration suggested using as targets the KB integrals at TBA mole fraction 0.04 and 0.10. The experimental KB integral of species TBA-TBA exhibits a global minimum at TBA mole fraction 0.04 and a global maximum at TBA mole fraction 0.10 (see squares in Figure 15). This feature is missing in the force field obtained after the third iteration (see rhomboids in Figure 15). Iteration IV produced a significant improvement over the whole concentration range. The force field produced by the fourth iteration (POP4ff) reproduces very well the three KB integrals over a wide concentration range (0.04-0.3), outperforming both OPLSUA and the force field developed by Lee and Van Der Vegt. The KB integrals for the different force fields as functions of the concentration are shown in figure 5. Note that only TBA mole fractions 0.2, 0.04, and 0.1 were used at any time in the optimization, leaving us ample data for meaningful testing.

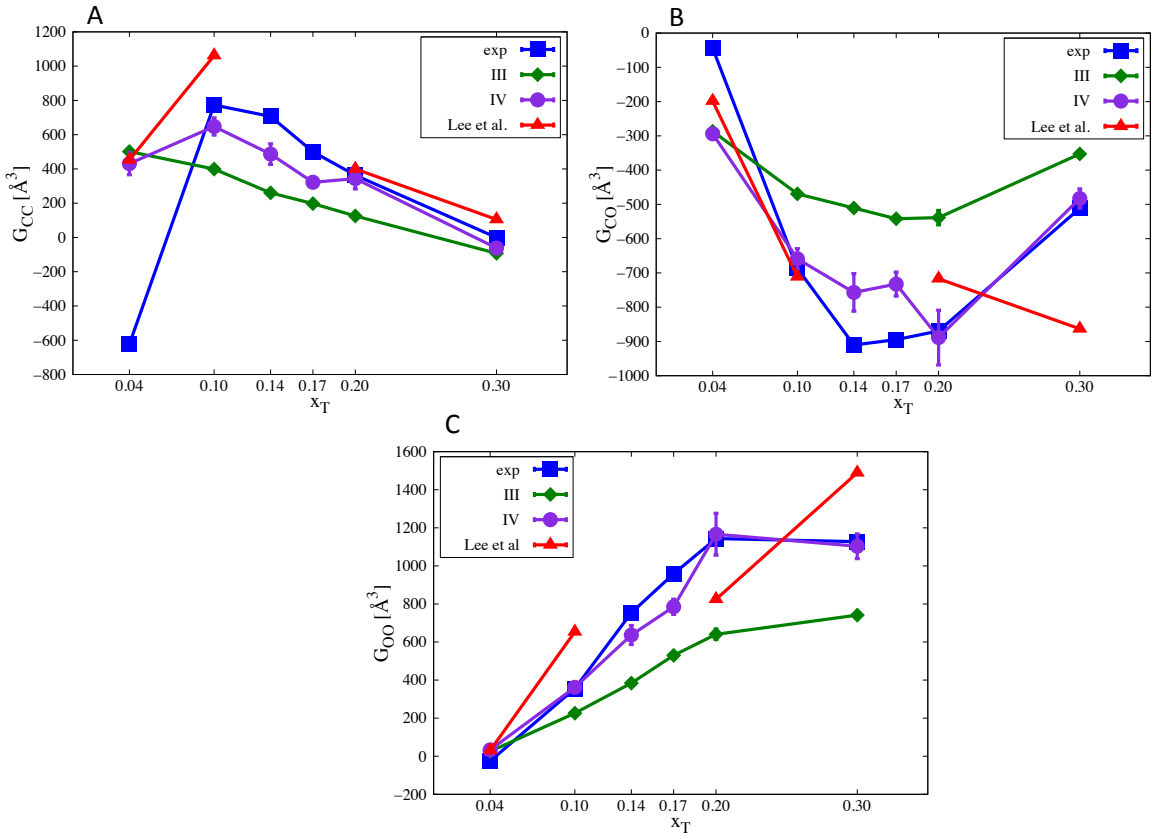

Figure 15: KB integrals as a function of TBA mole fraction. (A) TBA-TBA; (B) TBA-water; (C) water-water. Blue line shows the experimental results from [24], red line shows results from Lee and Van Der Vegt potential [21], green line shows computational results from force field POP3ff, and purple line shows computational results from force field POP4ff.

The pair correlation functions of TBA-TBA, TBA-water and water-water are shown in Figure 16. It is clear that the system is now well mixed because long-range correlations are absent. The pair correlation functions of TBA-TBA and TBA-water of OPLSUA (cyan in Figure 16) and POP4ff (purple in Figure 16) are significantly

different; OPLSUA shows two nearby peaks whereabouts POP4ff shows a single smooth peak. The pair correlation functions of force fields POP3ff (green in Figure 16) and POP4ff deviate only slightly. We did not include any information about the shape of the pair correlation functions in the target function; this change is a byproduct of the optimization procedure. Whether this is correct or not it is difficult to say since we do not know the pair correlation function from experiment, only its integral which hides such features.

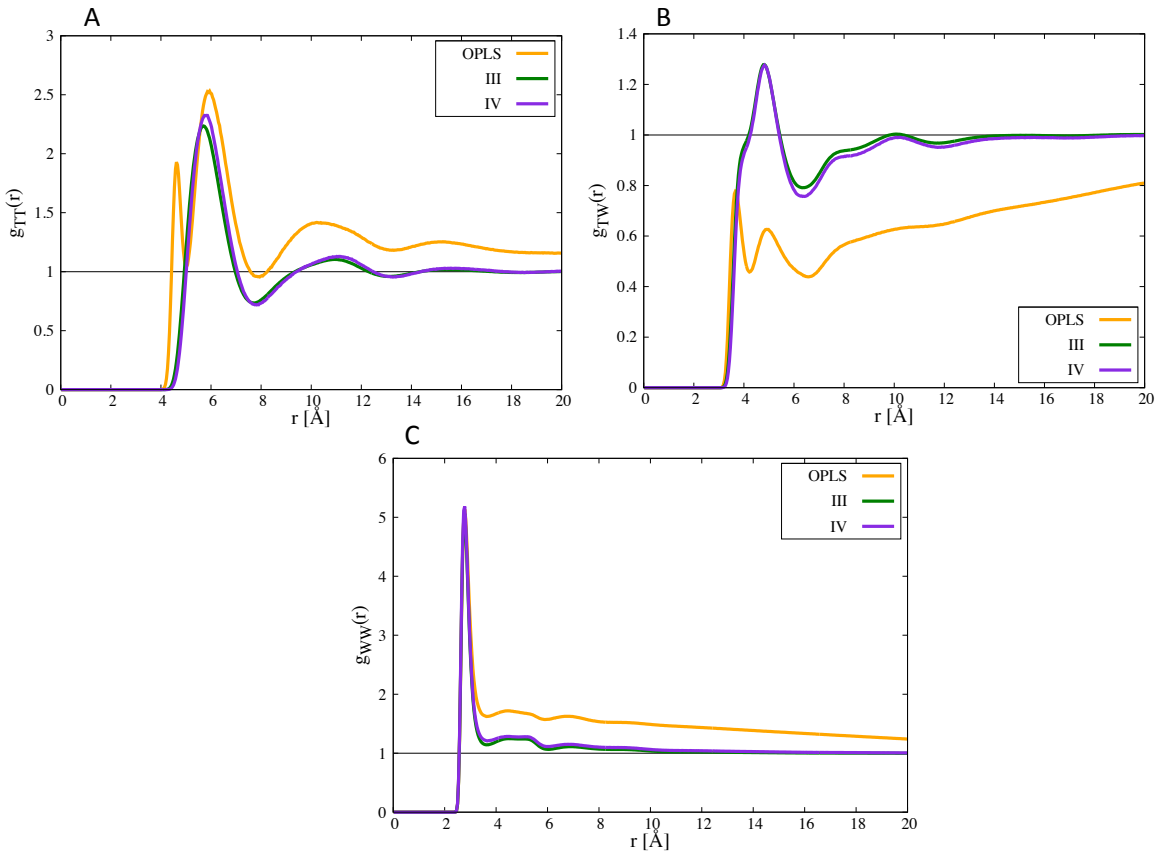

Figure 16: (A) pair correlation function for species TBA-TBA, yellow curve is the pair correlation function computed with the OPLS force field, green curve the pair correlation function computed with POP3ff, purple curve is the pair correlation function computed with force field POP4ff. (B) and (C) show the same information for species TBA-water and water-water. All the results are obtained at TBA mole fraction 0.20.

The different interaction types that are optimized at once do not contribute in the same way to the optimization. The sensitivity vector g is defined as the gradient in

parameter space of the target function in equation (4.14); it is a local feature of the target function and it changes as the optimization process improves the parameters set. To provide useful information, and following the procedure described in the Methods section, we multiply the gradient by the scaling matrix D^{-1} enforcing homogeneity in parameter space (see equation (2.9)). We also normalize the sensitivity vector. In Table 5 we report the 13 different components of the normalized and scaled sensitivity obtained after POP analysis of the simulations carried out with the OPLSUA parameters, i.e.

$$\frac{g}{|g|} = \frac{\nabla^T \Theta(\pi_{OPLSUA}) D^{-1}}{\left|\nabla^T \Theta(\pi_{OPLSUA}) D^{-1}\right|} \tag{4.17}$$

Torsion		
K_1	K_1	K_1
$1.9\ 10^{-5}$	$1.9\ 10^{-5}$	$1.9\ 10^{-5}$

Van der Waals A		
C	CH_3	O
$-6.5\ 10^{-3}$	$-4.2\ 10^{-2}$	$-3.0\ 10^{-2}$

Van der Waals B		
C	CH_3	O
$2.7\ 10^{-2}$	$1.1\ 10^{-1}$	$8.6\ 10^{-2}$

Charges			
C	CH_3	O	H
0.079	-0.86	0.36	0.31

Table 5: Scaled and normalized sensitivities (see eq.(4.17)) of the 13 parameters used in the optimization.

Initially, the KB integrals are insensitive to the torsions parameters, mildly sensitive to the LJ parameters (as was also noted by Lee and van der Vegt[21] by direct testing) and highly sensitive to the charge distribution.

It has been noted[71] that to properly mimic the behavior of liquid mixtures tuning only the dipole moment of the solute is not sufficient; it is required to find a solute charge distribution that represents higher order moments of the charge distribution. Indeed, we find that this distribution is the most important feature affecting the KB integrals.

The dipole moment of tert-butanol for OPLSUA is 2.28D and in our optimized force fields is 3.20D. The difference in dipole moment is the result of a redistribution of partial charges involving all the atoms; in OPLSUA the methyl groups are neutral and the positive charge is on the central carbon while in our potential the central carbon is almost neutral and each of the methyl groups carry a small positive charge [see Table 4].

After the third iteration and using a target function that includes information on two concentrations the sensitivity is significantly different. After the adjustment of the charge distribution the improved force field shows highest sensitivity to the LJ parameters. The last optimization step was indeed mainly a readjustment of the LJ parameters.

Finally, we extracted the angular dependence of the distribution of TBA and water around a central TBA molecule (see Fig. 17). The blue dots represent regions with high water density, the green dots regions with high TBA density. The figure is roughly symmetric for rotations of 120^{o} around the C-O axis of TBA. Because of steric repulsion, the high densities are in the grooves between these atoms. A region with high density of water is situated just under the methyl groups; contrary to what could be intuitive, the methyl groups, which are usually considered hydrophobic, are found well hydrated. Around the hydroxyl group, TBA tends to stay closer than water. Our model of TBA does not show hydrophobic interactions between methyl groups.

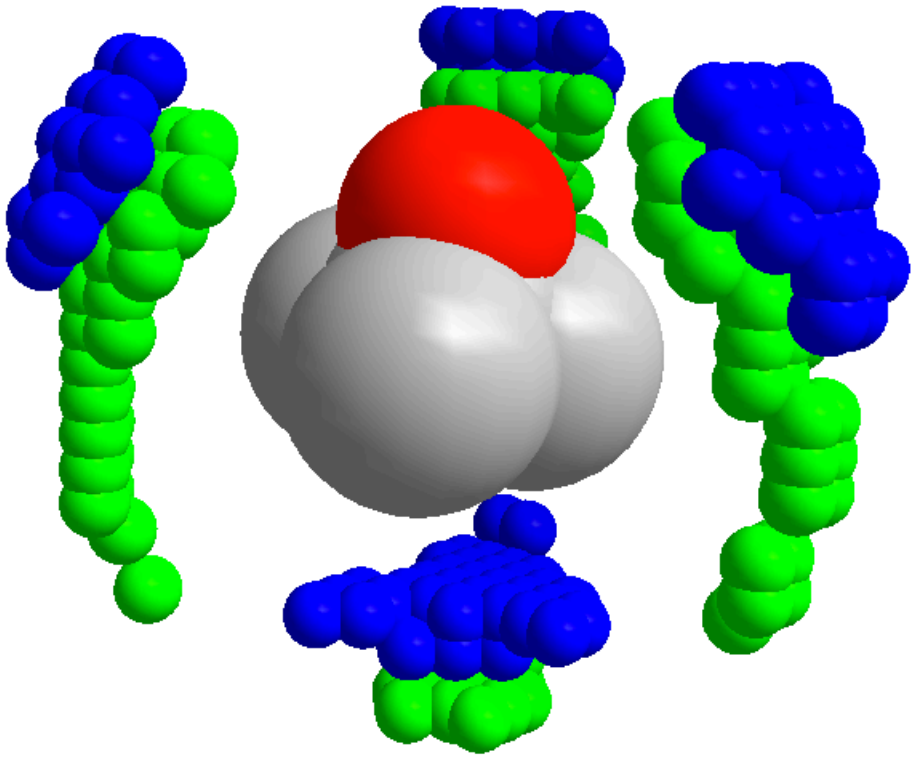

Figure 17: Regions with highest density of TBA (green) and water (blue) around a central TBA molecule. The densities are measured on a grid of size 0.5Å. As before, we assumed the position of the TBA molecule to be the position of the central carbon, and the position of the oxygen to represent the center of the water molecule. We color by green the cells that have a density of TBA larger than 85% of the maximum density of TBA measured. We color by blue the cells that have a density of water larger than 75% of the maximum density of water. The methyl groups are well hydrated as it is shown by the presence of a region of space with high density of water just under those groups. Methyl groups of TBA are also found close to the hydroxyl group of other TBA molecules. The presence of both water and TBA around both the hydroxyl group and the methyl groups indicates the absence of hydrophobic interactions between methyl groups.

On the uniqueness of the potential derived from KB integrals.

The optimization as described may depend on the initial conditions, producing potentials that are consistent with the experimental observables we examined but not unique. To explore the uniqueness of the potential, we conducted another optimization (we will refer to it as "control") starting from another set of parameters and for slightly different conditions.

Bond and angles parameters are left as is. The initial torsion parameters were the same as in OPLSUA (see Table 3). Also the initial charges were chosen to be the OPLSUA (see Table 4). The initial LJ parameters for the central carbon of TBA were set to (ε, σ)=(0.14450 kcal/mol, 3.96Å), while the initial ones of the methyl groups were set to (ε, σ)=(0.2940kcal/mol, 3.73Å). The initial LJ parameters for the oxygen and hydrogen of TBA's hydroxyl group were chosen to be the OPLSUA ones (see Table 4). We ran the same system as the one in table 2 for molar fraction of TBA 0.20, but with box size slightly larger ($65.505^3 Å^3$), corresponding to the average one found by Lee and van der Vegt for the same system.[21]The first run of this system showed a phase separation and the presence of a vacuum bubble in the periodic box.

The optimization was carried out with three iterations. At the beginning of each iteration, we ran 5ns of simulation using replica exchange algorithm,[30] [29] using 50 replicas equally spaced between 300K and 422.5K. After 1ns of equilibration, we collected 4000 structures, equally spaced in time, and run POP to optimize the force field parameters. In this case, we left the methyl groups uncharged, as it is originally in OPLSUA. At the second iteration, our protocol gave us a negative charge for the TBA hydrogen of the

hydroxyl group. We decided that such result was unphysical, so we discarded the optimization of the charge of the hydrogen atom at the second and third iteration. The final non-bonded parameters that we derived with this method are reported in the next table.

Non Bonded Parameters For Control and POP3ff

Atom Type	q (*e*)	ε (kcal/mol)	σ (Å)
C	0.04670 (0.45702)	0.0499 (0.1155)	3.8010 (4.0471)
CH_3	0.10920 (0)	0.1595 (0.0645)	3.9119 (4.3646)
O	-0.58180 (-0.56038)	0.1696 (0.5831)	3.0695 (2.5736)
H	0.20750 (0.10336)	0 (0)	0 (0)

Table 6: Non-bonded parameters for POP3ff; in brackets the parameters for control.

The charge distribution results in a dipole moment of 3.03D, slightly lower than the one found for the POP3ff and POP4ff (3.20D). The torsion parameters of the control optimization changed more than the POP3ff and POP4ff parameters. The final result is $(K_1, K_2, K_3)=(0.0019,-0.0032,0.5580)$.

The next figures show the pair correlation functions and the integral of the pair correlation functions for POP3ff and the result of the control optimization.

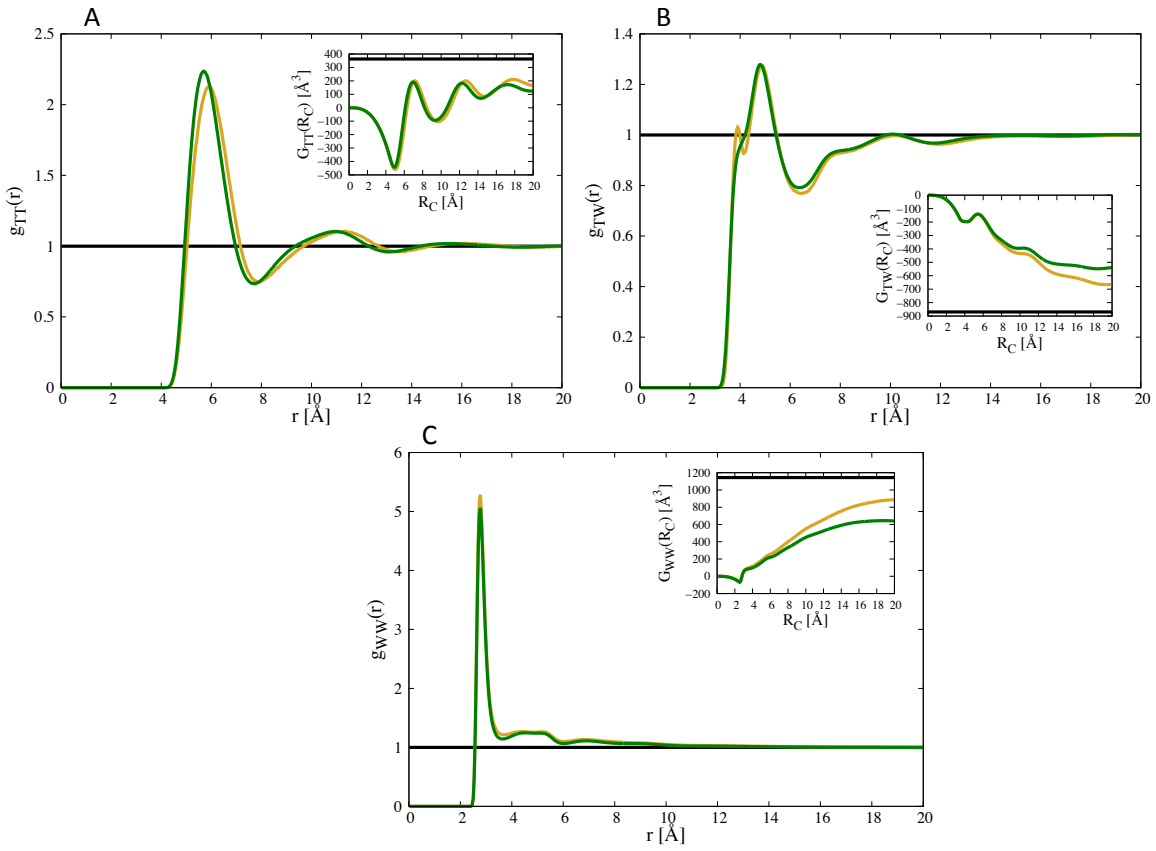

Figure 18: (A) pair correlation function of TBA-TBA; (B) TBA-water; (C) water-water. The green line represents POP3ff, the yellow line the control force field. In the insets, the KBIs are reported as a function of the cutoff distance. In black is shown the experimental value.

Even though we started from different parameters, we ran our simulations with a different optimization scheme (e.g. the methyl groups are left uncharged) and at a slightly different density, after the optimization we obtained for the KB integrals an accuracy similar to the one obtained with the POP3ff (see insets). The shape of the pair correlation

functions is remarkably close. The largest qualitative difference between the control (yellow) and the POP3ff (green) is perhaps in the first peak of the TBA-TIP3 pair correlation function for the control, which is missing in the POP3ff.

Both potentials are capable of reproducing the KBIs with comparable accuracy, and the pair correlation functions obtained with these two potentials are remarkably similar. This shows that the different potential can produce not only similar KB integrals but also similar pair correlation functions.

Conclusions

We provided a simple systematic procedure to optimize force fields to reproduce properties of liquid mixtures connected to the KB integrals.

We made a useful improvement to the original POP algorithm. The first version of POP was using Gradient Descent as a minimization algorithm. The introduction of Trust-Region Newton algorithm has improved the performance of POP in many ways. First of all, the Newton algorithm is known to have better convergence properties. Also, the concept of Trust-Region provides an easy and efficient way to assess the quality of the quadratic model used in the minimization. Finally, the use of a hyper-elliptical Trust-Region takes into account the different scales of magnitude present in the parameters set and allows modifications to the parameters that are homogeneous on a relative scale. We remark that the results shown in this chapter were achieved with just four iterations of parameter adjustments.

We developed a new force field for tert-butanol that approximates the behavior of mixtures of TBA with water better than force fields currently available as shown by comparison to the experimental KB values. In the first three iterations of the optimization we included in the target function only the KB integrals at one concentration (0.20 mole fraction of TBA). These iterations showed larger sensitivity towards the partial charges of TBA. In the last step of the optimization we included in the target function the KB integrals of two lower concentrations (0.04 and 0.10 mole fraction of TBA). In this case the charges, already optimized, did not change significantly, while most of the sensitivity was to LJ parameters. Even though our algorithm allowed for changes in torsional parameters, they remained essentially unchanged from the original OPLSUA parameters.

Lee and Van der Vegt[21] observed in the past that the KB integrals depend more on partial charge distribution than on LJ parameters. Similar observations were made in the context of Urea parameterization with KB integrals.[19] Our results for the first three iterations confirms, strengthens and quantifies these previous observations (see Table 5 for sensitivities to different force field parameters), as they are the consequence of an automated optimization of all the parameters at once. Nevertheless, we also observed that a fourth step of optimization of LJ parameters was necessary to improve the force field beyond what we obtained from the first three iterations (see Figure 15).

Lee and Van Der Vegt[21] used the GROMOS[72] force field, which has a more general (and complex) type of LJ interactions. The pair interactions parameters A_{ij} and B_{ij} are not separable to single atom parameters (i.e. $A_{ij} = A_i \cdot A_j$) but depends instead on both indices. We illustrate here that that the decomposable presentation, with a smaller number of parameters, works well. As a practical consequence we note that separating the pair interacting to one particle parameters make it possible to apply the Ewald sum for LJ interactions and to obtain more accurate description of long range forces.

Other differences between POP4ff force field and the force field developed by Lee and Van De Vegt[21] lie in the values of the parameters that in some cases are strikingly different; for example, the radius for the central carbon is ~6Å in the force field that they used, while in POP4ff the same carbon atom has a dimension that deviates only slightly from the original OPLS atom type (~4Å). The charge distribution is also very different, since they chose to keep the methyl groups neutral.

The fact that such diverse force fields produce similar results is a warning sign against optimizing liquid potentials solely according to KB data. The results are unlikely to be unique. This is also reflected in the comparison of two different potentials (POP3ff and control) reported in the previous section. Therefore, when we refine the parameters

using KB integrals, we need either to make sure that the changes to the force field are minimal, or to use a larger pool of observables to ensure compatibility towards other observables.

Finally we want to stress two important features of our optimization method. First, our method minimizes the target function with minimal changes to the parameter set. This is an important feature, given that force field parameters were already optimized extensively in the past. If we need to adjust these parameters against a new set of data, small adjustments are to be preferred since they are less likely to perturb results of previous refinement of the current set of potential parameters.

Second, our method does not require larger simulation time if the set of observables used for the optimization is increased. The change in the parameters is obtained as the post-processed analysis of one MD trajectory. This will make it easier and faster to optimize the force field against a larger pool of observables whenever such a large pool is available.

Conclusions

In this thesis, we developed a systematic reproducible approach toward the refinement of parameters for empirical energy functions for molecular simulations. This procedure, called POP, is a potentially useful approach for fine-tuning an energy function for applications in which statistical mechanics averages are compared with experimental measurements. The advantage of the proposed approach is that it can handle a large number of parameters in a single automated calculation. This is not to say that human decisions are completely factored out. Especially for cases in which multiple experimental observables are of interest, we expect to have weight coefficients for a sum of measured observables $\Theta = \sum_i w_i \left(\langle O_i \rangle - O_{\exp,i} \right)^2$ where the weights, w_i, are determined by the user. Experimental uncertainties as well as the importance of a particular observable for future projects impact the choice of the weights.

We showed that POP is very efficient in modifying the parameters of a force field so that target results are achieved; for all the applications in this manuscript, convergence was achieved in less than ten iterations. This is due to the use of the information contained in the gradient and to the fast-convergence properties of the Trust-Region Newton algorithm.

A secondary use of the software POP is toward the measurement of the sensitivity; by itself, the sensitivity does in fact supply useful insights about the physics of the system under investigation and about the properties of the model used.

A direction that we did not consider in this manuscript was to attempt a global optimization. While we argue that a global optimization is in general neither necessary nor useful, it may be of interest for some specific cases. One way to search for a global

minimum in an efficient way could be to combine the use of the sensitivity and stochastic sampling. The use of simulated tempering applied to the Langevin Equation in parameter space could constitute a very efficient sampling procedure to search for multiple solutions of parameter sets and potentially a global minimum of the target function.

We applied the POP algorithm to study the thermodynamics of peptides; specifically, we investigated the possibility to reproduce the melting curve by using the standard functional form of the energy function. We found that the equilibrium between the folded and unfolded state is very sensitive to the parameters in the force field and it can be adjusted quite efficiently by using POP. We also found that the temperature dependence of this equilibrium is instead quite insensitive to the choice of parameters and therefore we could not obtain a set of parameters that could reproduce experimental results for the pentapeptide WH5. Our result is similar to numerous previous attempts to reproduce the melting curve *in silico*; in fact, all attempts so far have had negative outcomes. Our negative result is indeed the strongest evidence suggesting that the current functional form of the force field cannot reproduce the temperature dependence observed in experiments. In order to provide this evidence, we performed the first full-space optimization for a midsize molecule. The dimensionality of our optimization was ~300, well beyond any previous example of force field refinement.

As a second application, we applied POP to the development of a force field for liquid mixtures. We applied the automated approach of POP to observables derived from the Kirkwood-Buff theory of mixtures and showed that our method is very efficient and produces accurate force fields. Starting from a force field that was clearly inaccurate, POP converged in five iteration steps to a final force field for the alcohol tert-butanol that approximates the behavior of its mixtures with water better than any other force field currently available.

Appendix: Explicit Calculation of Energy Derivatives

The complete potential is a sum of bonding and non-bonding terms:

$$U_{total} = \sum_{bonds} U_b + \sum_{angles} U_\theta + \sum_{\substack{improp \\ torsions}} U_{I\phi} + \sum_{torsions} U_\phi + \frac{1}{2} \sum_{\substack{i,j \in atoms \\ i \neq j}} U_{LJ} + \frac{1}{2} \sum_{\substack{i,j \in atoms \\ i \neq j}} U_{elec}$$

The functional form for bonded terms (bonds, angles, proper and improper torsions) is:

$$U_b = \frac{k_b}{2}\left(r - r_0\right)^2 \qquad U_\theta = \frac{k_\theta}{2}\left(\theta - \theta_0\right)^2$$

$$U_I = \frac{k_I}{2}\left(\phi_I - \phi_{I0}\right)^2 \qquad U_\phi = \sum_1^3 K_n \cos\left(n\phi + \delta\right)$$

The angle, bonds, and improper torsion potentials are not expected to require any condensed phase optimization; therefore, we do not report their derivatives.

The parameter δ is an arbitrary constant equal for all the torsion-types and is therefore not subject to optimization.

The non bonded terms (Lennard-Jones and electrostatic) are

$$U_{LJ} = 4\varepsilon_{ij}\left[\left(\frac{\sigma_{ij}}{r_{ij}}\right)^{12} - \left(\frac{\sigma_{ij}}{r_{ij}}\right)^{6}\right]$$

$$U_{elec} = k_{el}\frac{q_i q_j}{r_{ij}}$$

with combination rules:

$$\sigma_{ij} = \sqrt{\sigma_i \sigma_j} \qquad \varepsilon_{ij} = \sqrt{\varepsilon_i \varepsilon_j}\ .$$

Our software utilizes the equivalent formulation:

$$U_{LJ} = \left(\frac{A_i A_j}{r_{ij}^{12}}\right) - \left(\frac{B_i B_j}{r_{ij}^{6}}\right)$$

The vector of parameters π is a vector of dimension $3N_\phi + 3N_{atom}$ where N_ϕ is the number of torsion types and N_{atom} the number of atom types. Each torsion is in fact characterized by 3 parameters and each atom has two Lennard-Jones parameters and one charge.

There are n_i atoms of type i and n_ϕ torsions of type ϕ. The analytical gradient of the potential is the following:

$$\frac{dU}{dK_{1,\phi}} = \sum_{i=1}^{n_\phi} \cos\left(\phi_i + \delta\right)$$

$$\frac{dU}{dK_{2,\phi}} = \sum_{i=1}^{n_\phi} \cos\left(2\phi_i + \delta\right)$$

$$\frac{dU}{dK_{3,\phi}} = \sum_{i=1}^{n_\phi} \cos\left(3\phi_i + \delta\right)$$

$$\frac{dU}{dA_i} = \frac{1}{2} \sum_{l=1}^{n_i} \sum_{\substack{m=1 \\ m \neq l}}^{N} \frac{A_m}{r_{lm}^{12}}$$

$$\frac{dU}{dB_i} = -\frac{1}{2} \sum_{l=1}^{n_i} \sum_{\substack{m=1 \\ m \neq l}}^{N} \frac{B_m}{r_{lm}^{6}}$$

$$\frac{dU}{dq_i} = \frac{1}{2} \sum_{l=1}^{n_i} \sum_{\substack{m=1 \\ m \neq l}}^{N} \frac{q_m}{r_{lm}^{2}}$$

The only entries of the analytical Hessian matrix that are different from zero are:

$$\frac{d^2U}{dA_i dA_j} = \frac{1}{2} \sum_{l=1}^{n_i} \sum_{\substack{m=1 \\ m \neq l}}^{n_j} \frac{1}{r_{lm}^{12}}$$

$$\frac{d^2U}{dB_i dB_j} = -\frac{1}{2} \sum_{l=1}^{n_i} \sum_{\substack{m=1 \\ m \neq l}}^{n_j} \frac{1}{r_{lm}^{6}}$$

$$\frac{d^2U}{dq_i dq_j} = \frac{1}{2} \sum_{l=1}^{n_i} \sum_{\substack{m=1 \\ m \neq l}}^{n_j} \frac{1}{r_{lm}^{2}}$$

References

(1) Jorgensen, W. L.; Maxwell, D. S.; TiradoRives, J. *Journal of the American Chemical Society* **1996**, *118*, 11225.

(2) Verlet, L. *Physical Review* **1967**, *159*, 98.

(3) Frenkel, D.; Smit, B. *Understanding molecular simulation : from algorithms to applications*; 2nd ed.; Academic Press: San Diego, 2002.

(4) Tuckerman, M. *Statistical Mechanics and Molecular Simulations*; Oxford University Press, UK, 2008.

(5) MacKerell, A. D.; Bashford, D.; Bellott, M.; Dunbrack, R. L.; Evanseck, J. D.; Field, M. J.; Fischer, S.; Gao, J.; Guo, H.; Ha, S.; Joseph-McCarthy, D.; Kuchnir, L.; Kuczera, K.; Lau, F. T. K.; Mattos, C.; Michnick, S.; Ngo, T.; Nguyen, D. T.; Prodhom, B.; Reiher, W. E.; Roux, B.; Schlenkrich, M.; Smith, J. C.; Stote, R.; Straub, J.; Watanabe, M.; Wiorkiewicz-Kuczera, J.; Yin, D.; Karplus, M. *Journal of Physical Chemistry B* **1998**, *102*, 3586.

(6) Cornell, W. D.; Cieplak, P.; Bayly, C. I.; Gould, I. R.; Merz, K. M.; Ferguson, D. M.; Spellmeyer, D. C.; Fox, T.; Caldwell, J. W.; Kollman, P. A. *Journal of the American Chemical Society* **1995**, *117*, 5179.

(7) Shi, Y.; Xia, Z.; Zhang, J. J.; Best, R.; Wu, C. J.; Ponder, J. W.; Ren, P. Y. *Journal of Chemical Theory and Computation* **2013**, *9*, 4046.

(8) Savelyev, A.; MacKerell, A. D. J. *Journal of Computational Chemistry* **2014**, *35*, 1219.

(9) Mackerell, A. D. *Journal of Computational Chemistry* **2004**, *25*, 1584.

(10) Zhao, G. P.; Perilla, J. R.; Yufenyuy, E. L.; Meng, X.; Chen, B.; Ning, J. Y.; Ahn, J.; Gronenborn, A. M.; Schulten, K.; Aiken, C.; Zhang, P. J. *Nature* **2013**, *497*, 643.

(11) Shaw, D. E.; Maragakis, P.; Lindorff-Larsen, K.; Piana, S.; Dror, R. O.; Eastwood, M. P.; Bank, J. A.; Jumper, J. M.; Salmon, J. K.; Shan, Y. B.; Wriggers, W. *Science* **2010**, *330*, 341.

(12) Lange, O. F.; van der Spoel, D.; de Groot, B. L. *Biophys J* **2010**, *99*, 647.

(13) Di Pierro, M.; Elber, R. *J Chem Theory Comput* **2013**, *9*, 3311.

(14) Di Pierro, M.; Mugnai, M. L.; Elber, R. *The journal of physical chemistry. B* **2014**.

(15) Ruymgaart, A. P.; Cardenas, A. E.; Elber, R. *Journal of Chemical Theory and Computation* **2011**, *7*, 3072.

(16) Kirkpatrick, S.; Gelatt, C. D., Jr.; Vecchi, M. P. *Science* **1983**, *220*, 671.

(17) Lindorff-Larsen, K.; Maragakis, P.; Piana, S.; Eastwood, M. P.; Dror, R. O.; Shaw, D. E. *Plos One* **2012**, *7*.

(18) Kirkwood, J. G.; Buff, F. P. *J Chem Phys* **1951**, *19*, 774.

(19) Weerasinghe, S.; Smith, P. E. *Journal of Physical Chemistry B* **2003**, *107*, 3891.
(20) Weerasinghe, S.; Smith, P. E. *J Chem Phys* **2003**, *118*, 10663.
(21) Lee, M. E.; van der Vegt, N. F. A. *J Chem Phys* **2005**, *122*.
(22) Jorgensen, W. L. *J Phys Chem-Us* **1986**, *90*, 1276.
(23) Jorgensen, W. L.; Chandrasekhar, J.; Madura, J. D.; Impey, R. W.; Klein, M. L. *J Chem Phys* **1983**, *79*, 926.
(24) Nishikawa, K.; Kodera, Y.; Iijima, T. *J Phys Chem-Us* **1987**, *91*, 3694.
(25) Nocedal, J.; Wright, S. J. *Numerical optimization*; Springer: New York, 1999.
(26) More, J. J.; Sorensen, D. C. *Siam J Sci Stat Comp* **1983**, *4*, 553.
(27) Trefethen, L. N.; Bau, D. *Numerical linear algebra*; Society for Industrial and Applied Mathematics: Philadelphia, 1997.
(28) Kirkwood, J. G. *J Chem Phys* **1935**, *3*, 300.
(29) Marinari, E.; Parisi, G. *Europhysics Letters* **1992**, *19*, 451.
(30) Sugita, Y.; Okamoto, Y. *Chemical Physics Letters* **1999**, *314*, 141.
(31) Torrie, G. M.; Valleau, J. P. *J Comput Phys* **1977**, *23*, 187.
(32) Jorgensen, W. L.; Tiradorives, J. *Journal of the American Chemical Society* **1988**, *110*, 1657.
(33) Weiner, S. J.; Kollman, P. A.; Case, D. A.; Singh, U. C.; Ghio, C.; Alagona, G.; Profeta, S.; Weiner, P. *Journal of the American Chemical Society* **1984**, *106*, 765.
(34) Tuckerman, M.; Berne, B. J.; Martyna, G. J. *J Chem Phys* **1992**, *97*, 1990.
(35) Ruymgaart, A. P.; Elber, R. *Journal of Chemical Theory and Computation* **2012**, *8*, 4624.
(36) Ryckaert, J. P.; Ciccotti, G.; Berendsen, H. J. C. *J Comput Phys* **1977**, *23*, 327.
(37) Essmann, U.; Perera, L.; Berkowitz, M. L.; Darden, T.; Lee, H.; Pedersen, L. G. *J Chem Phys* **1995**, *103*, 8577.
(38) Jas, G. S.; Hegefeld, W. A.; Majek, P.; Kuczera, K.; Elber, R. *Journal of Physical Chemistry B* **2012**, *116*, 6598.
(39) Lin, M. M.; Mohammed, O. F.; Jas, G. S.; Zewail, A. H. *P Natl Acad Sci USA* **2011**, *108*, 16622.
(40) Hegefeld, W. A.; Chen, S. E.; DeLeon, K. Y.; Kuczera, K.; Jas, G. S. *J Phys Chem A* **2010**, *114*, 12391.
(41) Mohammed, O. F.; Jas, G. S.; Lin, M. M.; Zewail, A. H. *Angew Chem Int Edit* **2009**, *48*, 5628.
(42) Kaminski, G. A.; Friesner, R. A.; Tirado-Rives, J.; Jorgensen, W. L. *Journal of Physical Chemistry B* **2001**, *105*, 6474.
(43) Shalongo, W.; Dugad, L.; Stellwagen, E. *Journal of the American Chemical Society* **1994**, *116*, 8288.
(44) Vila, J. A.; Ripoll, D. R.; Scheraga, H. A. *P Natl Acad Sci USA* **2000**, *97*, 13075.

(45) Garcia, A. E.; Sanbonmatsu, K. Y. *P Natl Acad Sci USA* **2002**, *99*, 2782.
(46) Best, R. B.; Zhu, X.; Shim, J.; Lopes, P. E. M.; Mittal, J.; Feig, M.; MacKerell, A. D. *Journal of Chemical Theory and Computation* **2012**, *8*, 3257.
(47) Jorgensen, W. L.; Madura, J. D. *Mol Phys* **1985**, *56*, 1381.
(48) Mahoney, M. W.; Jorgensen, W. L. *J Chem Phys* **2000**, *112*, 8910.
(49) Ren, P. Y.; Ponder, J. W. *Journal of Physical Chemistry B* **2004**, *108*, 13427.
(50) Best, R. B.; Mittal, J. *Journal of Physical Chemistry B* **2010**, *114*, 14916.
(51) Abascal, J. L. F.; Vega, C. *J Chem Phys* **2005**, *123*.
(52) Mackerell, A. D.; Feig, M.; Brooks, C. L. *Journal of Computational Chemistry* **2004**, *25*, 1400.
(53) Best, R. B.; Mittal, J.; Feig, M.; MacKerell, A. D. *Biophys J* **2012**, *103*, 1045.
(54) Sakae, Y.; Okamoto, Y. *J Chem Phys* **2013**, *138*.
(55) Wu, J. C.; Chattree, G.; Ren, P. Y. *Theor Chem Acc* **2012**, *131*.
(56) Baker, C. M.; Anisimov, V. M.; MacKerell, A. D. *Journal of Physical Chemistry B* **2011**, *115*, 580.
(57) Ben-Naim, A. *Statistical thermodynamics for chemists and biochemists*; Plenum Press: New York, 1992.
(58) Chitra, R.; Smith, P. E. *J Chem Phys* **2001**, *114*, 426.
(59) Bennaim, A. *J Chem Phys* **1977**, *67*, 4884.
(60) Weerasinghe, S.; Smith, P. E. *J Chem Phys* **2003**, *119*, 11342.
(61) Weerasinghe, S.; Smith, P. E. *J Chem Phys* **2004**, *121*, 2180.
(62) Weerasinghe, S.; Smith, P. E. *Journal of Physical Chemistry B* **2005**, *109*, 15080.
(63) Ganguly, P.; van der Vegt, N. F. A. *Journal of Chemical Theory and Computation* **2013**, *9*, 1347.
(64) Mukherji, D.; van der Vegt, N. F. A.; Kremer, K.; Delle Site, L. *Journal of Chemical Theory and Computation* **2012**, *8*, 375.
(65) Fritsch, S.; Poblete, S.; Junghans, C.; Ciccotti, G.; Delle Site, L.; Kremer, K. *Phys Rev Lett* **2012**, *108*.
(66) Egorov, G. I.; Makarov, D. M. *J Chem Thermodyn* **2011**, *43*, 430.
(67) Nishikawa, K.; Hayashi, H.; Iijima, T. *J Phys Chem-Us* **1989**, *93*, 6559.
(68) Visser, C. D.; Perron, G.; Desnoyers, J. E. *Can J Chem* **1977**, *55*, 856.
(69) Kusalik, P. G.; Lyubartsev, A. P.; Bergman, D. L.; Laaksonen, A. *Journal of Physical Chemistry B* **2000**, *104*, 9533.
(70) Gallardo, I. F.; Webb, L. J. *Langmuir* **2012**, *28*, 3510.
(71) Ploetz, E. A.; Bentenitis, N.; Smith, P. E. *Fluid Phase Equilibr* **2010**, *290*, 43.
(72) Oostenbrink, C.; Villa, A.; Mark, A. E.; Van Gunsteren, W. F. *Journal of Computational Chemistry* **2004**, *25*, 1656.
(73) Berendsen, H. J. C.; Postma, J. P. M.; Van Gunsteren, W. F.; Hermans, J. In *Intermolecular Forces*; Springer Netherlands: 1981.